RESEARCH ARTICLE

Salt Adaptation in *Aegiceras Corniculatum*: Electrophysiology, Gene Expression, and Energy Trade-Offs

Jing Wang[1,†], **Mohamed Aboueldahab**[2,3,4,†], **Yanyou Wu**[2,*], **Deke Xing**[1,*] **and Qian Zhang**[1]

[1] School of Agricultural Engineering, Jiangsu University, Zhenjiang 212013, China
[2] State Key Laboratory of Environmental Geochemistry, Institute of Geochemistry, Chinese Academy of Sciences, Guiyang 550081, China
[3] University of Chinese Academy of Sciences, Beijing 100049, China
[4] Department of Botany and Microbiology, Faculty of Science, South Valley University, Qena 83523, Egypt

Abstract

The integration of physical and chemical processes underpins life. Plant cells function as bioelectrical units, storing and converting energy through capacitive, inductive, and resistive properties. This study elucidates the electrophysiological and molecular mechanisms governing salt transport and energy allocation in *Aegiceras corniculatum* leaves under combined salinity-waterlogging stress (T1: 0.1 M NaCl + 2 h; T2: 0.2 M NaCl + 4 h; T3: 0.4 M NaCl + 6 h). Results demonstrate that leaf intracellular water-salt transport dynamics, coupled with salt-transport gene expression, coordinately regulate active/passive transport, vacuolar compartmentalization, cytoplasmic Na^+ levels, and excretion. High salinity reduced salt excretion rate/capacity (LISTR/LISTC) and downregulated *SOS1*, while impairing water-holding capacity (LIWHC) and transport activities. Concurrent *VHAc1* upregulation elevated vacuolar H^+, inhibiting the Na^+/H^+ antiporter and compromising vacuolar salt sequestration. With increasing stress intensity, energy allocation shifted toward stress responses. Both electrical (internal) energy and ATP-derived chemical energy—originating from photosynthesis—jointly sustain plant vitality and adaptability; growth is primarily supported by internal energy, and adaptive differences dictate photosynthetic performance. This integrated analysis reveals how water-salt dynamics and molecular regulation confer salt tolerance in mangroves, offering insights crucial for coastal ecosystem resilience.

Keywords: *aegiceras corniculatum*, salt active transport, internal energy, photosynthesis, climate change.

1 Introduction

High sea levels can lead to the elevation of tidal foundation water levels, the intensification of coastal

Submitted: 18 September 2025
Accepted: 30 January 2026
Published: 12 February 2026

Vol. 1, **No.** 1, 2026.
10.62762/JPE.2025.184208

***Corresponding authors:**
✉ Yanyou Wu
wuyanyou@mail.gyig.ac.cn
✉ Deke Xing
xingdeke@ujs.edu.cn

† These authors contributed equally to this work

Citation
Wang, J., Aboueldahab, M., Wu, Y., Xing, D., & Zhang, Q. (2026). Salt Adaptation in *Aegiceras Corniculatum*: Electrophysiology, Gene Expression, and Energy Trade-Offs. *Journal of Plant Electrobiology*, 1(1), 7–31.

erosion, and the increase in saltwater intrusion [1]. Soil salinity and waterlogging, which covary with beach elevation within the tidal range, are key stress factors affecting mangrove plant growth, reproduction, and spatial distribution [2]. They can damage the functions of mangroves, such as absorbing water and ions and producing energy [3, 4]. These negative impacts have been reported for most species [5–7]. To resist salt and waterlogging stress, mangrove plants have evolved specialized adaptive characteristics, with intracellular ion compartmentalization being the most prominent. This process is crucial for maintaining intracellular ion homeostasis, osmotic balance, and membrane potential [8, 9].

Sodium ion (Na^+) is one of the key ions in plant homeostasis, and its transmembrane transport mechanisms vary according to the physiological state of the cells. In normal plant cells, with a low cytoplasmic concentration and a negative potential difference across the plasma membrane, the influx of Na^+ into plant cells occurs passively through channel proteins. It is directly driven by the electrochemical potential difference [10, 11]. Under high salt external conditions, plants activate active regulatory mechanisms to maintain low cytoplasm Na^+ concentration, such as sequestering Na^+ in the vacuole, limiting the amount of Na^+ initially entering the cell, or through active outflow of Na^+ from the cell into the plastid (via carrier proteins) [12, 13]. The above active transport processes are influenced by the activity of ion transporters on plasma and vacuolar membranes [14]. Numerous experimental studies have reported several critical signaling pathways involved in plant maintenance of intracellular Na^+ concentration. Halophytes can extrude Na^+ from the cytoplasm through the plasma membrane-located Na^+/H^+ antiporter or separate Na^+ into vacuoles through the vacuolar-located membrane Na^+/H^+ antiporter [8, 15]. The above signaling pathways are essential in salt compartmentalization and secretion [16, 17].

Furthermore, the secretion and compartmentation of Na^+ in plant cells are energy-dependent. They are usually stimulated by proton-driven H^+ flow coupling, such as plasma membrane H^+-ATPase and vacuolar membrane H^+-ATPase [18]. Maintenance of electrochemical H^+ gradients across the chromoplast and plasma membrane is crucial to these processes. When plants tolerate salt and hypoxia, ion transport is bound to cause energy consequences. Ion transport's total steady-state energy cost in Arabidopsis thaliana roots increases with the increase of external NaCl concentration [8]. Recent evidence indicates that pump activity may be inadequate to energize transport, especially under stress conditions [18]. The effects of these stresses on plants have been profoundly reflected at the molecular level. However, the behavior of the ions and electrons generated in this process, as well as the coupling relationship to the molecular mechanism, remains ambiguous and requires elucidation.

This ambiguity stems, in part, from the inherent limitations of relying solely on conventional molecular and biochemical approaches to capture the dynamic, integrated nature of plant stress adaptation. As summarized in Table 1, these limitations include the static and disruptive nature of most assays, the difficulty in quantifying the functional coupling between genes and physiology, the unresolved trade-offs between different adaptive mechanisms, the unclear patterns of energy allocation, and significant technical barriers in measuring real-time ion fluxes across membranes.

Plant electrophysiology serves as a viable measurement technique by providing a non-destructive, real-time window for characterizing the physiological requirements of plants in relation to environmental factors under specific conditions [19]. The electrical signal is a transient change of the potential gradient across the plasma membrane, and its excitation and conduction are usually related to the rapid response to environmental stimuli [20]. Plant cells have similar characteristics to those of inductance, originating from peripheral proteins and plant cell membrane binding proteins [21]. For instance, a single H^+ is transferred from the cytoplasm to the extracellular space by a proton pump on the plasma membrane, which creates an electric current using the energy released when ATP is converted into ADP and phosphate. When the proton pump pumps out H^+, it makes a potential and pH gradient on both sides of the membrane. This creates a proton electromotive force that turns ADP into ATP and weakens the current (Figure 1) [22, 23]. Surface (or peripheral) proteins constitute approximately 20 to 30% of membrane proteins, interacting with lipids on both sides of the membrane via charged amino acids or groups. In contrast, binding (or intrinsic) proteins account for approximately 70 to 80% of membrane proteins, interacting with lipids through hydrophobic hydroxyl groups within the membrane [24]. Surface proteins influence capacitive reactance and capacitance. Binding proteins influence inductive reactance and

Table 1. Multiple limitations using a single chemical response mechanism to explain the adaptation of mangrove plants to salinity.

Defect Type	Specific Description	Relevant References
Defects in static characterization	It can only provide "instant time-point" data on osmolytes, antioxidants, and gene expression, and cannot reflect real-time dynamic responses of the substances as mentioned above and related proteins.	-
Disruption of functional association	It is known that *NHX1* and *VHAc1* proton pumps synergistically participate in Na^+ sequestration, but their functional contributions to changes in vacuolar salt concentration cannot be quantified. It is difficult to directly establish a complete logical chain of "gene expression - ion transport - physiological adaptation".	[18, 32]
Lack of mechanism coupling	Na^+ sequestration mediated by the vacuolar membrane *NHX1* can maintain cell turgor, however, the direct correlation strength between this process and turgor maintenance cannot be determined. It is difficult to resolve the trade-off relationships and correlation degrees among cell turgor maintenance, reactive oxygen species (ROS) scavenging, and ion balance.	[33, 34]
Unclear energy allocation relationships	The synthesis of osmolytes, ion transport (for maintaining ion balance), and the scavenging of reactive oxygen species (ROS) all depend on cellular energy metabolism, but the patterns of energy allocation among these mechanisms remain unclear.	[35–37]
Technical threshold limitations	Existing technologies (e.g., Non-invasive Micro-test Technique (NMT), Nanoscale Secondary Ion Mass Spectrometry (NanoSIMS)) can measure certain indicators, but direct determination of ion fluxes across the plasma (or vacuolar) membrane remains extremely challenging. The prevailing ion balance mechanisms are merely speculative and require real-time online water-salt kinetic data for validation.	[38, 39]

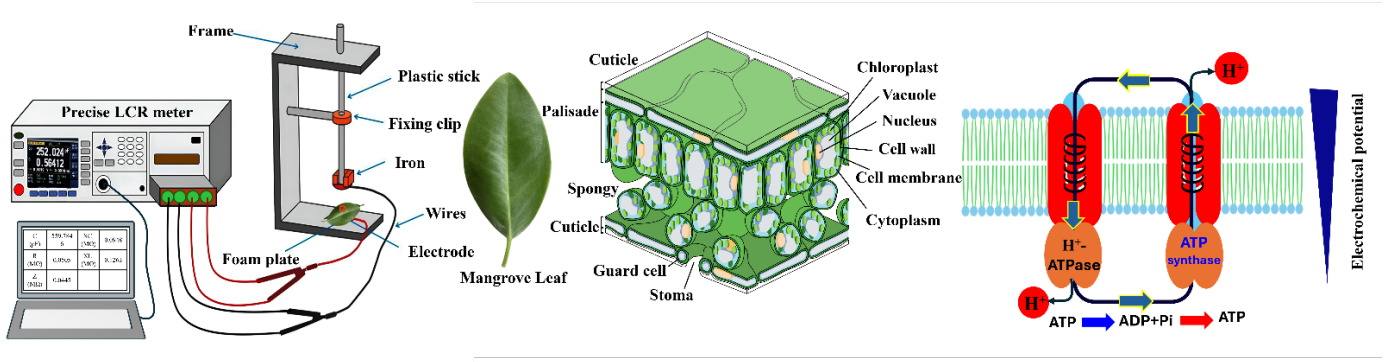

Figure 1. An LCR meter and a custom-built parallel plate capacitor were used to measure electrophysiological signals in plant leaves. Plant cells have the function of inductance, taking the proton pump on the plasma membrane as an example. The arrow on the pump indicates the direction of the current.

inductance. The concentration of these proteins on the cell membrane significantly affects the transport capacity of cellular components and, consequently, the plant's salt transport efficiency [25]. Among them, the proportion of binding proteins is closely related to the active transport of salt. Previous studies have shown that electrophysiological parameters can reflect ion transport dynamics. However, whether intracellular water-salt dynamic traits can mirror, and in what manner characterize, the functions of key water-salt transport genes in mangrove plants remains to be elucidated.

Internal energy in plant cells is stored as electrical energy within cellular electrical components and can be quantified using physiological capacitance

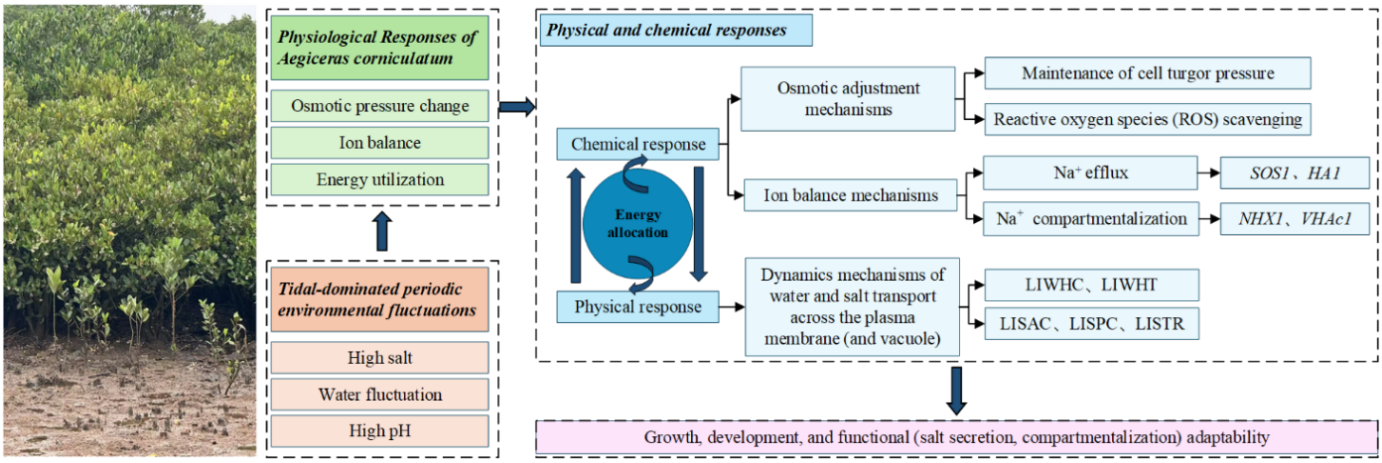

Figure 2. Effects of salinity on mangrove plants and their responses to salinity.

(C), resistance (R), impedance (Z), capacitive reactance (X_C), and inductive reactance (X_L), along with clamping force (F). Together, these electrophysiological parameters provide a useful real-time characterization of cellular internal energy status [26]. This internal electrical energy, along with chemical energy stored as ATP, ultimately derives from photosynthesis. Plants rely on both forms of energy to support biomass formation, sustain basic life processes, and respond to environmental stresses [27]. However, during mangrove adaption to salt stress, it remains unclear how photosynthetically derived energy is partitioned between chemical responses and physical responses? How do these two types of energy synergistically function in this process? These core mechanisms require further elucidation. In this study, *Aegiceras corniculatum*, a typical salt-secreting mangrove plant, was selected as an ideal model for studying the tolerance mechanism in halophytes. Although roots serve as the initial site for sensing changes in soil Na^+ concentration and osmotic pressure, playing a pioneering role in coordinating the overall stress response [28, 29], direct, continuous, and non-destructive physiological measurements of roots remain technically challenging. In contrast, leaves, as key organs for photosynthesis, energy conversion, and salt secretion, and their hydraulic traits directly influence plant water relations and stress acclimation capacity [30, 31]. Therefore, leveraging the advantages of leaves in physiological monitoring, this study characterizes the whole-plant physiological status by analyzing their electrophysiological responses, thereby investigating the systemic adaptation strategies of plants to environmental stress and elucidating the relationship between physical and chemical responses (Figure 2). Different salinity and waterlogging environments were simulated in the laboratory to examine the relationship between water-salt transport dynamics and salt transport-related gene expression of *A. corniculatum* under changing environmental conditions and to explore the transport mechanism of ions in plant leaves. This study aims to (i) elucidate the water-salt transport dynamics mechanism of the *A. corniculatum* in response to high salinity and waterlogging environments; reveal the dynamic and molecular-level synergistic processes of salt transport in the *A. corniculatum*. (ii) Explore the synergistic relationship between water-salt transport and gene expression in *A. corniculatum*, investigate the intrinsic links between water-salt transport and gene functions, and establish a model encompassing "Environmental (salt and waterlogging) stress perception—Gene expression coupled with water-salt transport—Salt transport dynamics—Physiological adaptation". (iii) Capture the characteristics of internal energy storage, conversion, and allocation in mangrove plants in response to environmental (salt and waterlogging) stress, integrate photosynthesis and growth, and explore the roles and contributions of chemical energy and different forms of internal energy in the environmental adaptation of mangrove plants.

2 Materials and Methods

2.1 Plant materials and treatments

The one-year-old *Aegiceras corniculatum* plants with uniform growth were used as experimental materials. All plant materials were provided by Quanzhou Tongqing Mangroves Technology Co. Ltd., Fujian, China. The experiments were conducted in the greenhouse of Jiangsu University (32°11′ N, 119°25′ E). The plants were cultivated under controlled environmental conditions with a relative humidity of 75 ± 5%, a day/night temperature regime of

30 °C/20 °C, and a photosynthetic photon flux density of 280 ± 10 μmol · m^{-2} · s^{-1}. Before experimental treatments, all plants were acclimated for one week using a half-strength Hoagland solution. The composition of the nutrient solution was as follows: 6 mmol · L^{-1} KNO_3, 4 mmol · L^{-1} $Ca(NO_3)_2$, 1 mmol · L^{-1} $NH_4H_2PO_4$, 2 mmol · L^{-1} $MgSO_4$, 2 μmol · L^{-1} KCl, 50 μmol · L^{-1} H_3BO_3, 5.3 μmol · L^{-1} $MnSO_4$, 4 μmol · L^{-1} $ZnSO_4$, 0.2 μmol · L^{-1} $CuSO_4$, 0.17 μmol · L^{-1} $(NH_4)_2MoO_4$, 0.04 mmol · L^{-1} EDTA-Na_2, and 0.04 mmol · L^{-1} $FeSO_4 \cdot 7H_2O$.

In natural coastal environments, mangrove growth is influenced by intertidal salinity and flood duration [40, 41]. These stress factors rarely occur independently; instead, they interact in complex ways to affect plant performance. Based on these ecological realities, three experimental treatments were established: T1 (0.1 M NaCl + 2 hours), T2 (0.2 M NaCl + 4 hours), and T3 (0.4 M NaCl + 6 hours). Salinity stress was applied by adding NaCl to the modified half-strength Hoagland solution, while a simulated tidal system [42] was used to control waterlogging duration. Following the acclimation period, NaCl concentration gradually increased daily over 7 consecutive days until the target salinity levels were achieved. The experimental treatments were then maintained for 60 days. During the treatment phase, tap water was added daily to maintain salinity, and the culture solution was reconfigured monthly to prevent algal contamination.

2.2 Growth index and leaf water potential Ψ_L

The height from top to ground of the plant was determined before and after the treatments using a meter scale (accuracy, 1 mm), and plant height increment (ΔH, cm) was calculated:

$$\Delta H = H_A - H_B \tag{1}$$

where H_A: Plant height after treatment; H_B: Plant height before treatment.

The leaf area was determined before and after the treatments using a LI-3000C Portable Leaf Area Meter (LI-COR, Lincoln, NE, USA), and leaf area increment (ΔL_A, cm^2) was calculated:

$$\Delta L_A = L_{AA} - L_{AB} \tag{2}$$

L_{AA}: Plant leaf area after treatment; L_{AB}: Plant leaf area before treatment.

After the treatment, the number of new leaves added (ΔL_N) was manually recorded. Leaf water potential (Ψ_L) was measured using a dew point water potential meter (C-52-SF Psypro, Wescor, Logan, Utah). The measurements at each treatment level were done in quintuplicate.

2.3 Electrophysiological parameters

2.3.1 *Determination of electrophysiological parameters*

After treating the plant for 60 days, the 3rd to 5th fresh, fully expanded leaves with uniform growth from top to bottom were selected. The leaf is added between the parallel electrode plates, and the diameter of the circular capacitor electrode plate is 7 mm. The LCR-6100 tester (GWINSTEK, Suzhou, China) is connected, and the parallel mode is used. The test voltage and frequency are 1.5 V and 3.0 kHz, respectively [43, 44]. Plant leaves' physiological impedance (Z), physiological resistance (R), and physiological capacitance (C) were measured by varying the clamping force using weights (100 g) under different pressures of 1.1 N, 2.1 N, 4.1 N, 6.1 N, and 8.1 N. These values were used to reflect the electrolyte concentration in the leaves and subsequently indicate the water, salt, and metabolic energy status of the leaf cells. Physiological capacitive reactance (X_c) and physiological inductive reactance (X_L) were calculated according to Equation 3 and 4 [45].

$$X_c = \frac{1}{2\pi f C} \tag{3}$$

$$\frac{1}{(-X_L)} = \frac{1}{Z} - \frac{1}{R} - \frac{1}{X_c} \tag{4}$$

where X_c is physiological capacitive reactance, π is 3.1416, f is frequency, C is physiological capacitance, X_L is physiological inductive reactance, Z is physiological impedance, and R is physiological resistance.

2.3.2 *Calculation of inherent electrophysiological parameters*

We have proved the internal mechanism relationship between clamping force (F) and plant leaves Z, R, X_c, X_L, and C based on the Gibbs free energy equation and Nernst equation, and the formulas were as follows [25]. The specific derivation formula can be found in the

supplementary file.

$$Z = y_1 + k_1 e^{-b_1 F} \quad (5)$$
$$R = y_2 + k_2 e^{-b_2 F} \quad (6)$$
$$X_c = y_3 + k_3 e^{-b_3 F} \quad (7)$$
$$X_L = y_4 + k_4 e^{-b_4 F} \quad (8)$$
$$C = y_0 + k_0 \quad (9)$$

where b_1 and k_1 are parameters of the Z fitting equation, b_2 and k_2 are parameters of the R fitting equation, b_3 and k_3 are parameters of the X_c fitting equation, b_4 and k_4 are parameters of the X_L fitting equation, y_0 and k_0 are parameters of the C fitting equation.

The clamping force and electrophysiological parameters (Z, R, X_c, and X_L) were fitted and analyzed using SigmaPlot 12.5 software to determine the intrinsic electrophysiological parameters of the plant leaves ($F = 0$) using the fitted equations. Inherent electrophysiological parameters include inherent impedance (IZ), inherent resistance (IR), inherent capacitive reactance (IX_c), and inherent inductive reactance (IX_L). The formulas were as follows:

$$IZ = y_1 + k_1 \quad (10)$$
$$IR = y_2 + k_2 \quad (11)$$
$$IX_c = y_3 + k_3 \quad (12)$$
$$IX_L = y_4 + k_4 \quad (13)$$

Plant leaves have electrical properties characterized by low capacitance and high resistance, which makes the inherent capacitance calculated using the fitting equation parameters susceptible to noise interference. Therefore, we use IX_c to calculate inherent capacitance (IC_p) according to Equation (14), which exhibits less fluctuation and is more stable and reliable:

$$IC_p = \frac{1}{2\pi f \times IX_c} \quad (14)$$

where $\pi : 3.1416$, f: the frequency.

The specific effective thickness (d) of the plant leaves can be calculated as:

$$d = \frac{U^2 k_0}{2} \quad (15)$$

2.3.3 *Calculation of inherent electrophysiological indexes*

Intracellular water use index and salt transport parameters. The intracellular water use index of plant leaves was calculated, including leaf intracellular water-holding capacity (LIWHC), leaf intracellular water-use efficiency (LIWUE), and leaf intracellular water-holding time (LIWHT) [45]. The calculation formulas were as follows:

$$\text{LIWHC} = (IC_p)^{\frac{3}{2}} \quad (16)$$
$$\text{LIWUE} = d/\text{LIWHC} \quad (17)$$
$$\text{LIWHT} = IC_p \times IZ \quad (18)$$

According to the methods described by Ali Solangi et al. [46] and Zhang et al. [45], we calculated several leaf intracellular salt transfer parameters: including leaf intracellular salt active transport capacity (LISAC), leaf intracellular salt passive transport capacity (LISPIC), leaf intracellular salt flux per unit area (LIUSF), leaf intracellular salt transfer rate (LISTR), and leaf intracellular salt transport capacity (LISTC). The corresponding calculation formulas were as follows:

$$\text{LISAC} = IX_L^{-1}/IR^{-1} \quad (19)$$
$$\text{LISPIC} = IX_C^{-1}/IR^{-1} \quad (20)$$
$$\text{LIUSF} = IR/IX_C + IR/IX_L \quad (21)$$
$$\text{LISTR} = (IC_p)^{\frac{3}{2}} / (IC_p \times IZ) \quad (22)$$
$$\text{LISTC} = \text{LIUSF} \times \text{LISTR} \quad (23)$$

Conduction capacity based on capacitive reactance and inductive reactance. The physiological current is generated by the movement of dielectric substances (including inorganic and organic ions) within leaves. This current reflects the conductivity of polar substances and is directly correlated with the leaf's hydraulic conductivity. The biological significance of conduction capacity based on physiological current can be characterized by the change of physiological current under unit pressure, representing the conductivity of leaves [47].

X_c reflects the ability to resist physiological currents. Similarly, the inherent conduction capacity of plant leaves based on IX_c (ICC_{XC}) was obtained:

$$ICC_{XC} = \frac{U b_3 k_3}{(y_3 + b_3)(y_3 + b_3)} \quad (24)$$

The biological meaning of this formula is to reflect the transport capacity of "capacitive" dielectric substances in leaves, especially the passive transport capacity

and the charging and discharging capacity of the cell membrane.

The resistance of an inductor to current is referred to as inductive reactance. Similar to ICC_{XL}, the inherent conduction capacity of plant leaves based on IX_L (ICC_{XL}) was obtained:

$$ICC_{XL} = \frac{Ub_4k_4}{(y_4 + b_4)(y_4 + b_4)} \tag{25}$$

The biological meaning of the above formula is to reflect the transport capacity of "inductive" dielectric substances in leaves, especially the active transport capacity of the cell membrane.

Conduction resistance based on capacitive reactance and inductive reactance. The Z of leaves reflects their ability to oppose physiological currents. As the Z increases, the transport of these substances slows down. Therefore, the Z of leaves can reflect the conductivity of polar substances in leaves from the opposite aspect, which is also the hydraulic conduction ability of leaves. The biological significance of the inherent conduction resistance of plant leaves based on Z can be characterized by the change of physiological impedance under unit pressure, representing the conductive resistance based on Z in leaves of the plant [47].

Similarly, according to the derivation formula of the relationship model between X_c and F:

$$X_c' = -b_3k_3e^{-b_3F} \tag{26}$$

The X_c of plant leaves reflects the ability to resist physiological currents, while physiological currents are generated by the transport of "**capacitive**" dielectric substances. The biological meaning of the above formula can be characterized as the change of X_c under unit pressure, which represents the conduction resistance of plant leaves based on X_c. When $F = 0$, the value is the inherent conduction resistance of plant leaves based on X_c (ICR_{XC}):

$$ICR_{XC} = X'_{C_{F=0}} = -b_3k_3 \tag{27}$$

Compared to the ICR_{XC} of different plant leaves, the greater the transport resistance, the more challenging it is for "**capacitive**" dielectric substances to be transported, resulting in a slower transport rate.

Similar to X_c, according to the derivation formula of the relationship model between X_L and F:

$$X_L' = -b_4k_4e^{-b_4F} \tag{28}$$

The X_L of plant leaves also reflects the ability to resist physiological currents, while physiological currents are generated by the transport of "**inductive**" dielectric substances. Similarly, when $F = 0$, the value is the inherent conduction resistance of plant leaves based on X_L (ICR_{XL}):

$$ICR_{XL} = X'_{L_{F=0}} = -b_4k_4 \tag{29}$$

Compared to the ICR_{XL} of different plant leaves, the higher the value, the more difficult it is to transport the "**inductive**" dielectric substances.

Unit cellular internal energy and cellular internal energy. According to the method described by Duan et al. [26], the unit cellular internal energy based on Z (ΔG_{Z-E}) and R (ΔG_{R-E}) of plant leaves was calculated:

$$\Delta G_{Z-E} = \frac{\ln k_1 - \ln y_1}{b_1} \tag{26}$$

$$\Delta G_{R-E} = \frac{\ln k_2 - \ln y_2}{b_2} \tag{27}$$

Similar to the derived formulas for ΔG_{R-E} and ΔG_{Z-E}, unit cellular internal energy based on X_C (ΔG_{XC-E}) is obtained.

$$\Delta G_{XC-E} = \frac{\ln k_3 - \ln y_3}{b_3} \tag{28}$$

Similar to the derived formula of ΔG_{X-C-E}, the unit cellular internal energy based on X_L (ΔG_{XL-E}) is obtained.

$$\Delta G_{XL-E} = \frac{\ln k_4 - \ln y_4}{b_4} \tag{29}$$

Cellular internal energy was calculated based on unit cellular internal energy and specific effective thickness (d), including cellular internal energy based on Z (ΔG_Z), cellular internal energy based on R (ΔG_R), cellular internal energy based on X_C (ΔG_{XC}), and cellular internal energy based on X_L (ΔG_{XL}). The formulas are as follows:

$$\Delta G_Z = \frac{\ln k_1 - \ln y_1}{b_1} \times d \tag{30}$$

$$\Delta G_R = \frac{\ln k_2 - \ln y_2}{b_2} \times d \tag{31}$$

$$\Delta G_{XC} = \frac{\ln k_3 - \ln y_3}{b_3} \times d \tag{32}$$

$$\Delta G_{XL} = \frac{\ln k_4 - \ln y_4}{b_4} \times d \tag{33}$$

2.4 Photosynthetic parameters

After 60 days of treatment, photosynthetic parameters were measured on the third and fifth fully expanded leaves. The net photosynthetic rate (P_N, $\mu mol\,m^{-2}\,s^{-1}$), stomatal conductance (g_s, $mol\,m^{-2}\,s^{-1}$), and transpiration rate (E, $mmol\,m^{-2}\,s^{-1}$) were recorded using a portable Li-6400XT Photosynthesis Measurement System (LI-COR, Lincoln, NE, USA). Furthermore, the instantaneous water use efficiency (WUE_i, $\mu mol\,mmol^{-1}$) was calculated. All measurements were performed in quintuplicate for each treatment level. The WUE_i was calculated formula as follows:

$$WUE_i = P_N/E \tag{34}$$

2.5 ATP content

After 60 days of treatment, the plant's third and fifth fully unfolded fresh leaves were extracted, immediately frozen in liquid nitrogen, and stored at -80°C in a refrigerator. For the measurement of ATP content, fresh leaf samples (0.1 g) were homogenized and processed using an ATP Content Assay Kit (Solarbio, Beijing, China) in accordance with the manufacturer's guidelines. The final total ATP concentration was normalized to the fresh weight of the tissue and was expressed as μmol/g FW. Crucially, all stages of the homogenization and extraction workflow were conducted on ice to suppress enzyme activity and ensure the stability of ATP.

2.6 Gene expression

Frozen tissue was ground using a mortar and pestle, and total RNA was isolated from leaves using the RNAprep Pure Plant Total RNA Extraction Kit (Tiangen Biochemical Technology Co. Ltd., Beijing, China). RNA was quantified with 260 nm and 280 nm readings, and integrity was verified by ethidium bromide-stained formaldehyde gel analysis. Total RNA reverse transcribed into DNA using the FastKing RT Kit with gDNA Eraser (Tiangen Biochemical Technology Co. Ltd., Beijing, China). The specific primer sequences of PM Na^+/H^+ antiporter (*SOS1*), vacuolar Na^+/H^+ antiporter (*NHX1*), PM H^+ ATPase (*HA1*) and vacuolar H^+-ATPase subunit c (*VHAc1*) are shown in Table 2 [17]. Furthermore, the 18S rRNA was used as the reference gene. Subsequently, Quantitative real-time PCR (qRT-PCR) was performed using cDNA and FastReal qPCR PreMix (SYBR Green) (Tiangen Biochemical Technology Co. Ltd., Beijing, China) in an ABI StepOnePlus™ Real-Time PCR System (Applied Biosystems, Waltham, USA). All reactions were carried out in a 20 µL final volume containing 10 µL 2×FastReal qPCR PreMix (SYBR Green), 0.6 µL each of forward and reverse primers, 1 µL of cDNA, and 2 µL 50× ROX Reference Dye, and nuclease-free water to a total volume of 20 µL. Relative quantification values for each target gene were calculated by the $2^{-\Delta\Delta C_t}$ method.

Table 2. Primers of *SOS1*, *NHX1*, *HA1*, *VHAc1*, and *18S rRNA* genes for real-time quantitative PCR.

Primer name	Primer sequence (5′~3′)
SOS1-F	GGCTGAAGACGGAATCGGAGGT
SOS1-R	ATGAGGAGGGCGACGGTGTATG
NHX1-F	CGTCGGTGGTTCTTTTCAAT
NHX1-R	AAAGGTACGCCATGAGCATC
HA1-F	AAGTCCACGGCATTATCGAC
HA1-R	CATGCCTAGGAGGGTCAAAA
VHAC1-F	GTAGCCTCGATGGGTGTGAT
VHAC1-R	AATGCCAATAGCCATTCCAG
18S rRNA-F	TTCCTTGTAAGCGCGAGTCA
18S rRNA-R	ATCCGAACACTTCACCGGAC

2.7 Statistical Analysis

All datasets were evaluated for normality using the Shapiro-Wilk test and for homogeneity of variances using Levene's test. All variables satisfied the normality assumption ($p > 0.05$). However, Levene's test indicated that the electrophysiological dataset violated the assumption of homoscedasticity, whereas all other datasets met this criterion. Accordingly, data were analyzed using one-way analysis of variance (ANOVA). For the electrophysiological data, post hoc pairwise comparisons were conducted using Tamhane's T2 test; for all other data, Duncan's multiple range test was used. For significant overall ANOVA effects, partial eta squared (η_p^2) is reported with its 95% confidence interval (95% CI). For all post hoc pairwise comparisons, Cohen's d is reported with its 95% CI. Pearson correlation coefficients were also computed. A p-value ≤ 0.05 was considered statistically significant. All statistical analyses and figures were performed using R Statistical Software (v4.4.3; R Core Team 2025) and Origin 2022 (OriginLab, Northampton, MA, USA).

Subsequently, using T1 treatment as the control, relative values for the T2 and T3 treatments were calculated as follows:

$$R_i = \frac{M_i}{C_i} \tag{39}$$

where R_i is the relative value of variable i, M_i is its measured value under treatment, and C_i is its

corresponding control value (T1 treatment).

Based on Equation (39), the following relative metrics were derived:

- Relative ATP content per unit fresh weight (R_{ATP}) from ATP content per unit FW
- Relative unit cellular internal energy (R_{UCIE}) from $\Delta G_{\mathrm{XL-E}}$
- Relative growth-driving energy (R_{GDE}) from the specific effective thickness d

These relative quantities were then used to quantify the energy allocation trade-off through the conservation relation:

$$R_{\mathrm{ATP}} + R_{\mathrm{UCIE}} = R_{\mathrm{GDE}} + R_{\mathrm{SRE}} \tag{40}$$

where R_{SRE} denotes the derived relative stress-response energy.

Similarly, to assess the trade-off between growth and adaptation, the following relative metrics were calculated:

- Relative photosynthesis (R_{P}) from net photosynthetic rate P_N
- Relative cellular internal energy (R_{CIE}) from ΔG_{XL}
- Relative growth (R_{G}) from plant height increment ΔH

These metrics were related by:

$$R_{\mathrm{P}} + R_{\mathrm{CIE}} = R_{\mathrm{G}} + R_{\mathrm{AE}} \tag{41}$$

where R_{AE} is the derived relative adaptive efficiency.

3 Results

3.1 Effects of treatments on growth indices and leaf water potential (Ψ_L).

The ΔH decreased with increasing salinity and prolonged waterlogging duration; however, the value for the T1 treatment was markedly more significant than that for the T2 ($t(8) = 4.17$, $p = 0.003$, Cohen's $d = 0.65$, 95% CI [0.83, 4.37]) and T3 treatments ($t(8) = 5.43$, $p = 0.001$, Cohen's $d = 0.56$, 95% CI [1.33, 5.46]). Nonetheless, there was a negligible change in the ΔL_A across each therapy ($F(2, 12) = 0.78$, $p = 0.479$, $\eta_p^2 = 0.12$, 95% CI [0.00, 0.37]).

The ΔL_N exhibited a significant disparity ($F(2, 12) = 248.22$, $p < .001$, $\eta_p^2 = 0.98$, 95% CI [0.92, 0.99]), with the peak recorded value occurring during the T1 therapy. The Ψ_L value of T2 was slightly elevated compared to that of T3 ($t(8) = 1.44$, $p = 0.187$, Cohen's $d = 0.09$, 95% CI [-0.43, 2.20]) (Table 3).

Table 3. Increment of plant height, leaf area, number of new leaves, and water potential under different treatments.

Treatments	T1	T2	T3
ΔH (cm)	3.45±0.24^{a}	1.73±0.34^{b}	1.53±0.26^{b}
ΔL_A (cm^2)	7.02±0.45^{a}	7.92±0.71^{a}	7.31±0.34^{a}
ΔL_N	33.00±1.53^{a}	13.33±0.67^{b}	1.33±0.67^{c}
Ψ_L (Mpa)	–1.20±0.03^{b}	–1.06±0.04^{a}	–1.14±0.04^{ab}

Note: mean ±SE (n=5), the same letter in the same row indicates no significant difference ($p > 0.05$) according to one-way ANOVA followed by Duncan's multiple range test.

3.2 Effects of treatments on electrophysiological parameters

The LIWHC at T1 treatment was significantly higher than other treatments (T2: $t(4.22) = 7.72$, $p = 0.001$, Cohen's $d = 4.88$, 95% CI [2.20, 7.51]) (T3: $t(4.04) = 7.78$, $p = 0.001$, Cohen's $d = 4.92$, 95% CI [2.22, 7.56]). In contrast, the LIWUE at T3 treatment was significantly higher than T1 treatment ($t(7.36) = -4.04$, $p = 0.004$, Cohen's $d = -2.56$, 95% CI [-4.26, -0.77]). The LIWHT values at the T1 and T2 treatments did not differ significantly ($t(5.66) = -1.36$, $p = 0.226$, Cohen's $d = -0.86$, 95% CI [-2.14, 0.47]) but both were markedly lower than this value at the T3 treatment (T1: $t(7.56) = -14.18$, $p < .001$, Cohen's $d = -8.97$, 95% CI [-13.44, -4.48]) (T2: $t(6.52) = -7.93$, $p < .001$, Cohen's $d = -5.02$, 95% CI [-7.70, -2.28]).

The value of LISAC increased with the increase of salinity and waterlogging time. The values of LISPC and LIUSF showed the same trend as those of LISAC. The calculation of LISAC / LIUSF and LISPIC / LIUSF showed that passive transport had a slight advantage in salt transfer compared with active transport. This phenomenon was more evident during the T3 treatment. With the increase in salinity and waterlogging time, the LISTR value gradually decreased. The law of LISTR was consistent with that of LISTC.

The ΔG_{Z-E}, ΔG_{R-E} and ΔG_{XC-E} showed slight increases with increasing treatment intensity, though differences were not statistically significant. The ΔG_{XL-E} increased with escalating salinity and waterlogging severity, with significantly higher values in T3 compared to T1 treatments ($t(5.34) = -3.53$, $p = 0.015$, Cohen's $d = -2.23$, 95% CI [-3.83, -0.55]). The d value was significantly higher in T1 compared to T2 ($t(8.00) = 5.79$, $p < .001$, Cohen's $d = 3.66$, 95% CI [1.47, 5.78]) and T3 ($t(4.98) = 7.94$, $p = 0.001$, Cohen's $d = 5.02$, 95% CI [2.28, 7.71]). Similarly, the ΔG_Z at T1 treatment was significantly higher than other treatments (T2: $t(7.96) = 3.07$, $p = 0.016$, Cohen's

Table 4. Leaf intracellular water use indices, salt transfer parameters, (unit) cellular internal energy, specific effective thickness, conductance capacity, and conduction resistance under different treatments.

Treatments		T1	T2	T3
Leaf intracellular water use indices	LIWHC	387.94 ± 42.71	53.72 ± 7.11	54.87 ± 3.17
	LIWUE	0.06 ± 0.01	0.20 ± 0.08	0.15 ± 0.02
	LIWHT	14.68 ± 1.15	18.39 ± 2.47	41.24 ± 1.48
Leaf intracellular salt transfer parameters	LISAC	0.25 ± 0.02	0.30 ± 0.04	0.66 ± 0.03
	LISPIC	0.29 ± 0.03	0.38 ± 0.06	1.25 ± 0.12
	LIUSF	0.54 ± 0.04	0.68 ± 0.09	1.91 ± 0.14
	LISTR	27.11 ± 3.66	2.97 ± 0.26	1.33 ± 0.06
	LISTC	14.17 ± 1.58	1.98 ± 0.27	2.53 ± 0.20
	LISAC / LIUSF	46.14%	44.69%	34.48%
	LISPIC / LIUSF	53.86%	55.31%	65.52%
Unit cellular internal energy	ΔG_{Z-E}	1.84 ± 0.17	2.12 ± 0.48	2.89 ± 0.30
	ΔG_{R-E}	1.74 ± 0.28	1.97 ± 0.52	2.54 ± 0.23
	ΔG_{XC-E}	1.96 ± 0.11	2.63 ± 0.32	3.71 ± 0.54
	ΔG_{XL-E}	1.90 ± 0.11	2.46 ± 0.34	2.95 ± 0.27
	$\Delta G_{XL-E}/\Delta G_{XC-E}$	96.94%	93.54%	79.51%
Cellular internal energy	ΔG_Z	42.01 ± 5.11	19.00 ± 5.49	22.42 ± 1.56
	ΔG_R	39.14 ± 7.19	17.91 ± 5.62	19.78 ± 1.28
	ΔG_{XC}	45.4 ± 5.24	22.36 ± 4.54	29.67 ± 5.54
	ΔG_{XL}	43.8 ± 5.01	21.22 ± 4.76	23.29 ± 2.57
	$\Delta G_{XL}/\Delta G_{XC}$	96.47%	94.93%	78.49%
Specific effective thickness	d	42.01 ± 5.11	19.00 ± 5.49	22.42 ± 1.56
Conductance capacity	ICC_{XC}	39.14 ± 7.19	17.91 ± 5.62	19.78 ± 1.28
	ICC_{XL}	45.4 ± 5.24	22.36 ± 4.54	29.67 ± 5.54
	ICC_{XC}/ICC_{XL}	86.16%	80.10%	66.67%
Conduction resistance	ICR_{XC}	-0.52 ± 0.11	-2.06 ± 0.78	-1.39 ± 0.30
	ICR_{XL}	-0.56 ± 0.10	-2.24 ± 0.74	-3.07 ± 0.42
	ICR_{XC}/ICR_{XL}	92.86%	91.96%	45.28%

$d = 1.94$, 95% CI [0.35, 3.45]) (T3: $t(4.74) = 3.66$, $p = 0.016$, Cohen's $d = 2.32$, 95% CI [0.61, 3.95]). The ΔG_R value of the T2 treatment was the smallest. The ΔG_{XC} values at T2 ($t(7.84) = 3.32$, $p = 0.011$, Cohen's $d = 2.10$, 95% CI [0.46, 3.67]) and T3 ($t(7.98) = 2.06$, $p = 0.073$, Cohen's $d = 1.31$, 95% CI [-0.12, 2.66]) treatments were significantly lower than that at T1 treatment. The trend of ΔG_{XL} was consistent with that of ΔG_{XC}. The value of $\Delta G_{XL}/\Delta G_{XC}$ was the smallest under T3 treatment. At T1 treatment, the ICC_{XC} was the highest. However, the value of ICC$_{XL}$ decreased significantly with increasing salinity and waterlogging time ($F(2, 12) = 144.392$, $p < .001$, $\eta_p^2 = 0.96$, 95% CI [0.87, 0.97]). The treatments did not have a remarkable effect on the ICR_{XC} ($F(2, 12) = 2.48$, $p = 0.125$, $\eta_p^2 = 0.29$, 95% CI [0, 0.54]), but the ICR_{XL} increased with it, and the resistance was the highest at the T3 treatment. The ICC_{XC} / ICC_{XL} values increased gradually with salinity and waterlogging time, while ICR_{XC} / ICR_{XL} values decreased gradually (Table 4).

3.3 Effects of treatments on photosynthetic parameters

The P_N had the highest value at the T2 treatment and the lowest at the T3 treatment. The value of g_s at the T2 treatment was significantly higher than at the T3 treatment ($t(8) = 2.48$, $p = 0.038$, Cohen's $d = 0.04$, 95% CI [0.08, 2.98]). Although the value of E displayed an insignificant variation between T1 and T2 ($t(8) = -0.08$, $p = 0.941$, Cohen's $d = 1.44$, 95% CI [-1.29, 1.19]), it was significantly lower at the T3 treatment compared to T1 ($t(8) = 2.63$, $p = 0.030$, Cohen's $d = 1.19$, 95% CI [0.15, 3.11]). The value of WUE_i was considerably lower at the T1 treatment than at other treatments (T2: $t(8) = -3.62$, $p = 0.007$, Cohen's $d = 0.14$, 95% CI [-3.91, -0.59]) (T3: $t(8) = -4.31$, $p = 0.003$, Cohen's $d = 0.19$, 95% CI [-4.49,

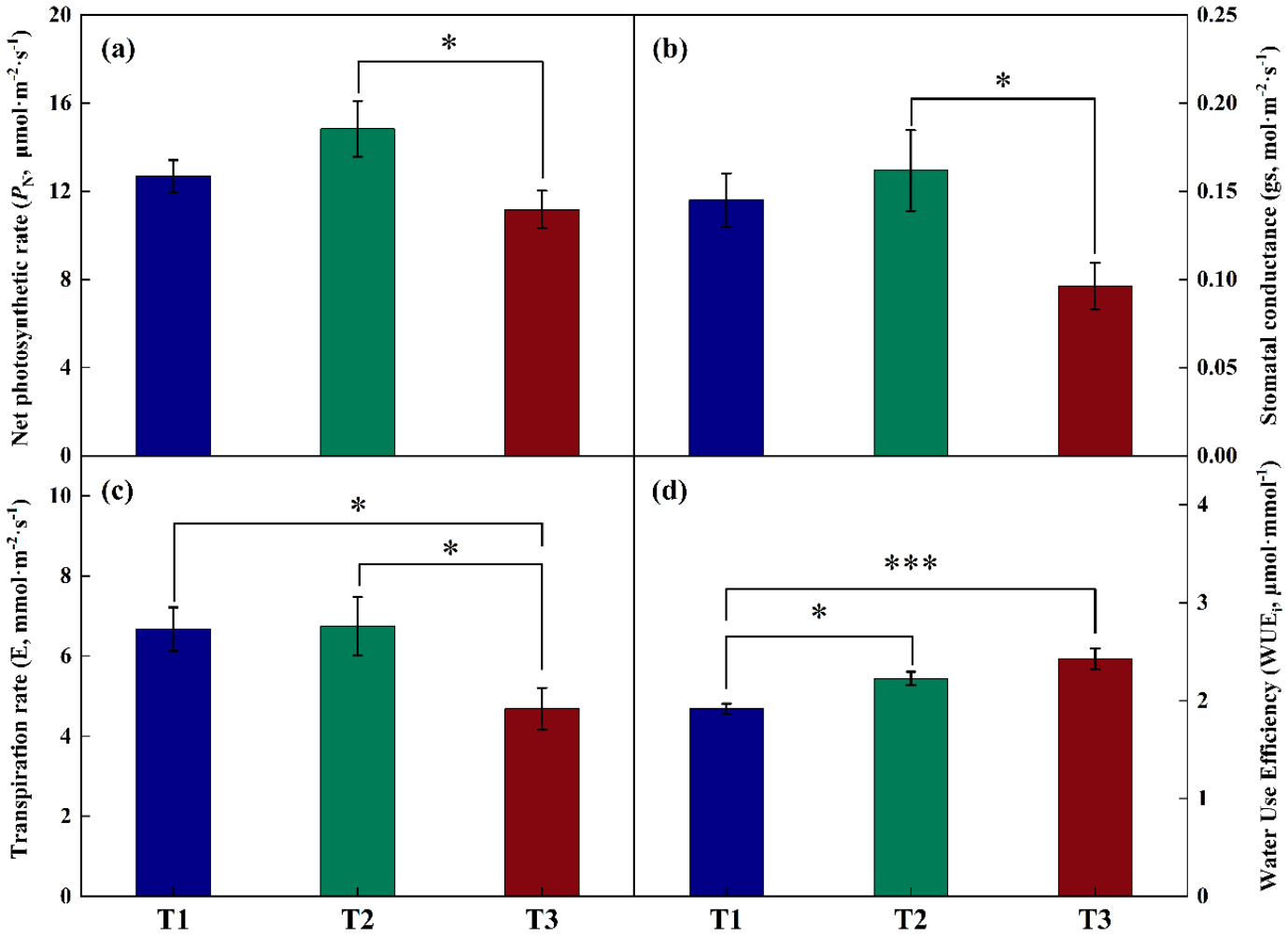

Figure 3. Changes in photosynthetic characteristics under different treatments. Statistical significance is denoted as: ***p < 0.001, **p < 0.01, *p < 0.05, according to one-way ANOVA followed by Duncan's multiple range test, n = 5..

-0.88]) (Figure 3).

3.4 Effects of treatments on ATP content

ATP content increased dependently with the increase of salinity and waterlogging time (F (2, 12) = 93.58, p < .001, ηp^2 = 0.94, 95% CI [0.80, 0.96]) (Figure 4).

3.5 Effects of treatments on gene expression

With the increase in salinity and waterlogging time, the expression of the *SOS1* gene was down-regulated ($F(2, 12) = 8.22$, $p = 0.006$, $\eta_p^2 = 0.58$, 95% CI [0.09, 0.74]). The *NHX1* expression at the T3 treatment was considerably lower than at the T1 treatment ($t(8) = 3.38$, $p = 0.010$, Cohen's $d = 0.30$, 95% CI [0.49, 3.71]). The expression of *HA1* was the lowest at T2 treatment. However, the expression of *VHAc1* increased significantly with increasing salinity and waterlogging time ($F(2, 12) = 24.56$, $p < .001$, $\eta_p^2 = 0.80$, 95% CI [0.44, 0.88]). Among them, the *VHAc1* gene expression of T2 and T3 treatments was 4.57 and 11.12 times that of T1 treatment, respectively (Figure 5).

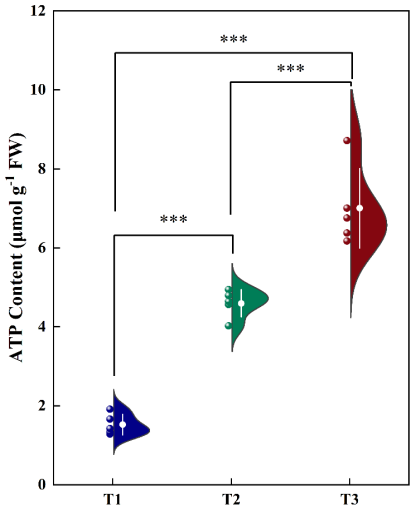

Figure 4. Change of ATP content under different treatments. Statistical significance is denoted as: ***p < 0.001, **p < 0.01, *p < 0.05, according to one-way ANOVA followed by Duncan's multiple range test, n = 5.

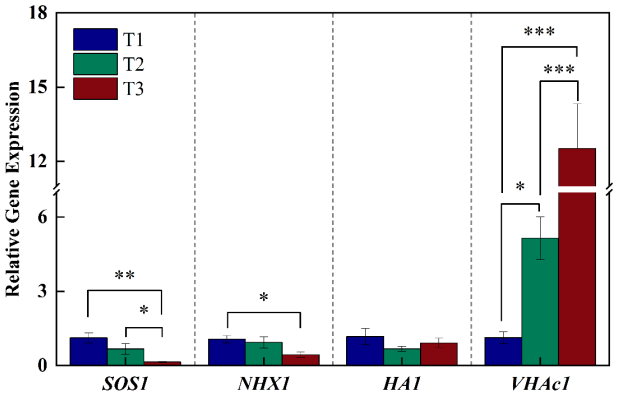

Figure 5. Relative gene expression levels of Na^+/H^+-antiporter and H^+-ATPase in the plasma membrane and vacuole membrane of leaves under different treatments. The relative expression levels of each gene were standardized with *18S rRNA* as the internal reference gene. Statistical significance is denoted as: ***p < 0.001, **p < 0.01, *p < 0.05, according to one-way ANOVA followed by Duncan's multiple range test, n = 5.

3.6 Correlation analysis and Principal component analysis results

To integrate the diverse physiological, electrophysiological, and molecular variables and identify the main axes of response to salinity-waterlogging stress, we conducted Pearson correlation analysis and principal component analysis (PCA) on the complete dataset. ΔG_{Z-E} was significantly and positively correlated with LIWHT, LISAC, LISPIC, LIUSF, ATP, and *VHAc1*; ΔG_{R-E} was significantly positively correlated with LISPIC and LIUSF; ΔG_{XC-E} and ΔG_{XL-E} were significantly positively correlated with LIWHT, LISAC, LISPIC, LIUSF, ATP, and *VHAc1*, and negatively correlated with ΔL_N, LIWHC, LISTR, ICC_{XC}, and ICC_{XL}. ATP showed a highly significant positive correlation with LIWHT, LISAC, LISPIC, LIUSF, and *VHAc1*, and significant negative correlations with ΔH, ΔL_N, LIWHC, LISTR, LISTC, ICC_{XC}, ICC_{XL}, ICR_{XL}, *SOS1*, and *NHX1* (Figure 6(a)).

The first three principal components together explained 77.32% of the total variance. Variables related to water utilization, salt transport, conductance capacity, and conduction resistance showed high loadings on these components, indicating that these trait groups serve as representative factors reflecting physiological indicators of the *A. corniculatum* under different treatments (Figure 6(b)).

3.7 Energy allocation and trade-offs in *Aegiceras corniculatum*

To elucidate the energy allocation characteristics of physiological processes in *Aegiceras corniculatum* during environmental adaptation and to quantify the trade-off between cell *turgor* maintenance and ion homeostasis, we used T1 treatment as the control treatment and expressed T2 and T3 relative values. The calculation results are shown in Table 5.

Using T1 as the control, R_{ATP} increased as treatment intensity escalated. R_{UCIE} showed a progressive increase, rising from 1 to 1.29 and then to 1.55 with increasing treatment severity. In contrast, R_{GDE} declined to 0.37 and 0.35 as treatment intensity increased. From these observations, the "Energy Reserve-Stress Response-Growth" model was developed: $R_{ATP} + R_{UCIE} = R_{GDE} + R_{SRE}$. Using this model, R_{SRE} was calculated, increasing from 1 to 3.92 and then to 5.78 as the treatment intensity escalated.

R_P reached a maximum of 1.17 under T2 and declined to 0.88 under T3. In both T2 and T3, R_{CIE} was reduced to approximately 50% of the control (T2: 0.48, T3: 0.53). R_G exhibited highly synchronous change with relative cellular internal energy (T2: 0.50, T3: 0.44). On this basis, we formulated the "Photosynthetic Energy-Internal Energy-Growth-Adaptation" model was constructed: $R_P + R_{CIE} = R_G + R_{AE}$. Using this framework, R_{AE} was calculated, reaching 1.15 in T2 and dropping to 0.97 in T3, thereby paralleling the trend in relative photosynthesis.

4 Discussion

4.1 Intracellular water-salt dynamic characteristics can characterize the real-time physical responses of mangrove plants to salinity and waterlogging

The survival of mangrove plants at the land-sea interface continues to be profoundly constrained by environmental factors, notably salinity and the duration of waterlogging [48]. *A. corniculatum* employs dual strategies for Na^+ homeostasis: salt glands [49] and intracellular regulation [16, 50]. While ions normally interact with water to form relatively stable hydrated shells, thereby contributing to osmotic balance and cell turgor, salinity and waterlogging stress disrupt this equilibrium by altering both external ion concentrations and internal water status [51]. High external Na^+ elevates the driving force for passive Na^+ influx, whereas waterlogging-induced

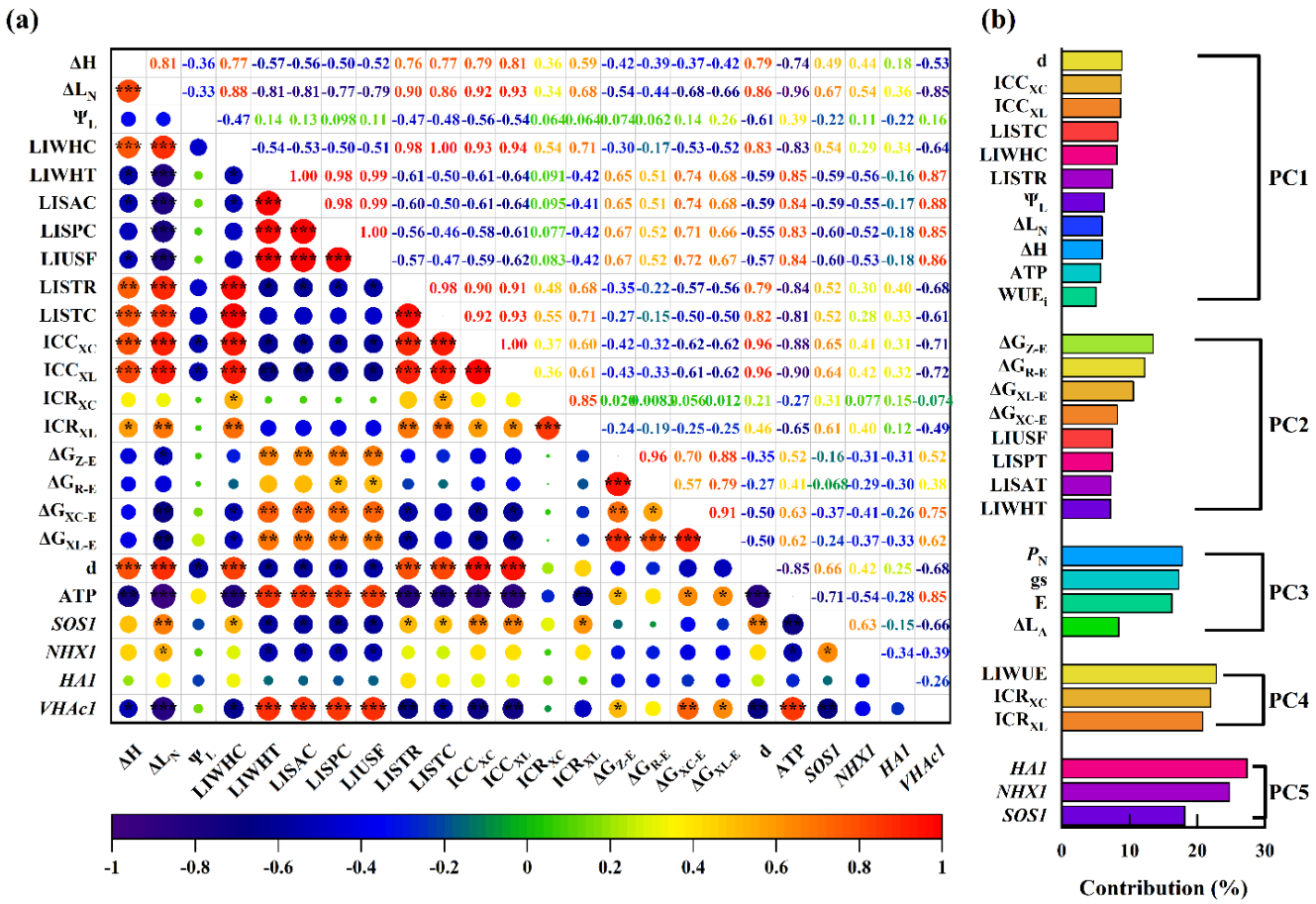

Figure 6. Correlation analysis and principal component analysis (PCA) of A. corniculatum under different treatments. (a) Correlation matrix of water utilization, salt transport, unit cellular internal energy, ATP content, and gene expression. Color intensity corresponds to the magnitude of the Pearson correlation coefficient (red for positive and blue for negative correlations). Statistical significance is denoted as: ***p < 0.001, **p < 0.01, *p < 0.05. (b) is a PCA estimate based on the complete data set, showing the contribution of each variable to the retained principal components (PCs). Among them, only variables whose absolute load value is greater than 0.6 are retained. Cumulative variance explained by the first three PCs is shown in parentheses (PC1: 50.98%, PC2: 68.26%, PC3: 77.32%, PC4: 84.28%, PC5: 89.02%).

hypoxia restricts root metabolism and ATP production, thereby constraining active ion transport and vacuolar compartmentalization. As a result, maintaining Na^+ homeostasis under combined salinity-waterlogging conditions requires a coordinated adjustment of salt gland activity, intracellular ion partitioning, and water–salt transport dynamics across tissues [52]. At T1, LIWHC was maximal, the intracellular water was sufficient, and the water and salt flow inside and outside the cells was smooth. Conversely, T3 (severe stress) induced a significant increase in LIUSF and LIWHT, but a decrease in LIWHC and LISTR, ultimately leading to a substantial reduction in the compartmentalization ability of the vacuoles and prolonged exposure of the cytoplasm to high concentrations of salt. The chemical potential difference for Na^+ across the plasma membrane was significantly enhanced by the electrical potential difference, as demonstrated by the Nernst equation [53]. This steep electrochemical potential gradient results in the passive influx of Na^+ into the cell. Concurrently, the active efflux is driven by the electrochemical H^+ gradient generated by the plasma membrane proton ATPase [54]. Therefore, intracellular sodium ion levels are determined by passive influx along the electrochemical gradient and active efflux along the counter-electrochemical gradient [55]. In this study, compared with T1 treatment, both LISAC and LISPC of T3 significantly increased, but LISAC/LISPC significantly decreased from 0.86 to 0.53; correspondingly, both ICC_{XC} and ICC_{XL} of T3 significantly decreased, but ICC_{XC}/ICC_{XL} increased dramatically from 116.10% to 186.49%. This indicates that in T3 treatment, the passive influx is markedly greater than the active efflux, leading to a decrease in the salt excretion capacity and a significant increase in salt ions within the cytoplasm in *A. corniculatum*.

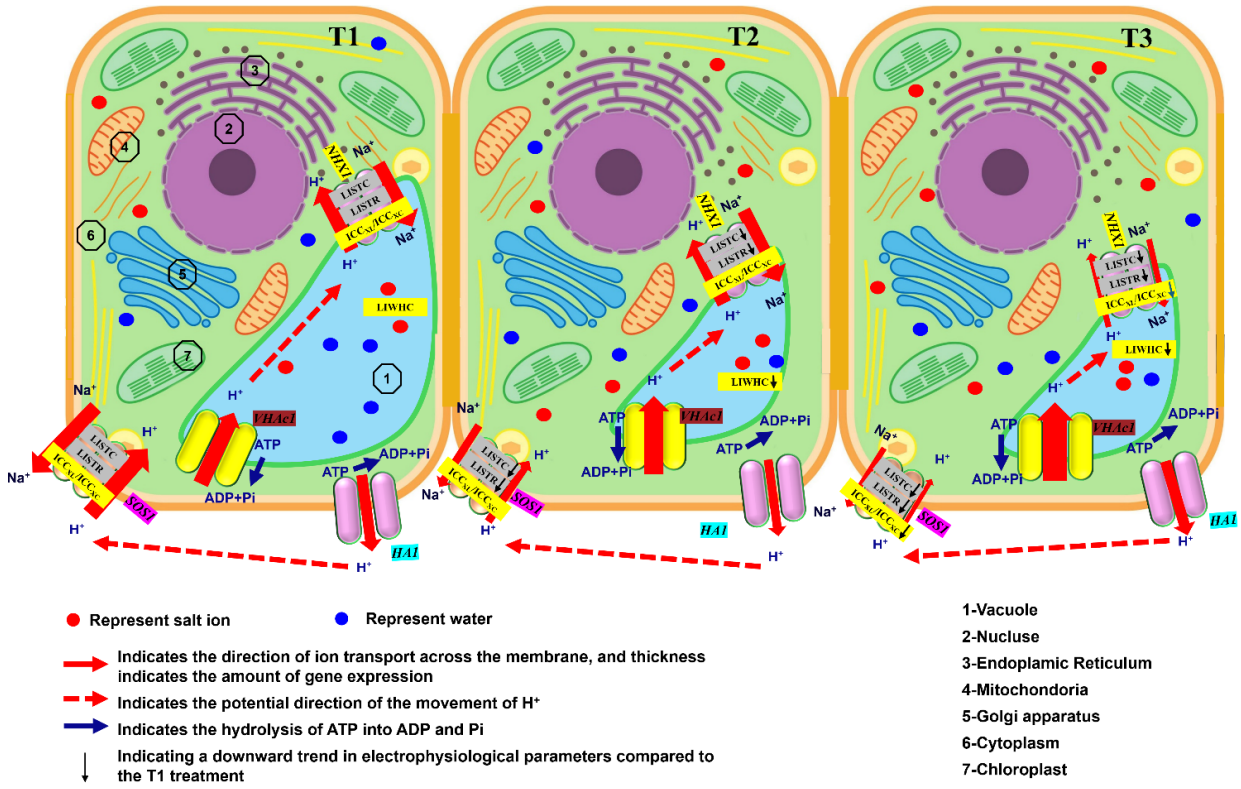

Figure 7. The internal relationship between intracellular electrophysiological characteristics and Na^+ transport-related genes in leaves of *A. corniculatum* under different treatments.

Table 5. Energy partitioning dynamics under salinity-waterlogging stress: Trade-offs between growth and adaptation.

Treatments	T1	T2	T3
R_{ATP}	1.00	3.00	4.58
R_{UCIE}	1.00	1.29	1.55
R_{GDE}	1.00	0.37	0.35
R_{SRE}	1.00	3.92	5.78
R_P	1.00	1.17	0.88
R_{CIE}	1.00	0.48	0.53
R_G	1.00	0.50	0.44
R_{AE}	1.00	1.15	0.97

4.2 The expression of key water-salt transport genes in mangrove plants is closely coupled with intracellular water-salt transport dynamics

Building on the water-salt transport dynamics described in subsection 4.1, we next examined whether these biophysical changes correspond to alterations in the activity of genes responsible for salt transport and compartmentalization. Our results revealed that *SOS1* was downregulated, whereas *VHAc1* experienced a significant upregulation as salinity and waterlogging stress increased in *A. corniculatum*. Compared to the T1 treatment, the T3 treatment markedly upregulated *VHAc1* expression, elevating vacuolar H^+ concentration and reducing pH, which compromised *NHX1*-mediated Na^+ vacuolar sequestration. The concurrent downregulation of *SOS1* expression impaired plasma membrane Na^+ efflux capacity. This suggested that there was a synergistic decrease in active transmembrane transport efficiency of Na^+ in leaf cells, ultimately disrupting both cytoplasmic Na^+ homeostasis and vacuolar compartmentalization.

The gene expression are indicative of adaptations to alterations in water-salt transport dynamics. When comparing the T2 and T3 treatments to T1, there was a notable downregulation of *SOS1* and an upregulation of *VHAc1*. However, this was accompanied by a significant decrease in LISTR and ICC_{XC} (ICC_{XL}), and a significant increase in LISPC / LISAC and $\Delta G_{XC-E}/\Delta G_{XL-E}$. There was no significant difference in *NHX1* expression between T2 and T1, and consequently, LISAC and LISPC were not significantly impacted. In contrast, when comparing T3 to T1, *NHX1* expression was downregulated, and correspondingly, LISAC and LISPC were significantly increased. Collectively, these patterns support the view that the salt excretion capacity and vacuolar

salt compartmentalization capacity of *A. corniculatum* are jointly regulated by genes associated with salt transport and water-salt transport dynamics.

In addition, although P_N of T2 and T3 was less affected, both LISTR and LISTC were significantly reduced. This decrease in the water-salt transport rate ultimately resulted in a significant slowdown in plant growth. Thus, it is evident that water-salt transport dynamics also serve as an endogenous driving force for the survival and growth of plants (Figure 7). Overall, our findings suggest that electrophysiology-based water-salt dynamics indicators can serve as an important basis for verifying the functions of genes related to water-salt transport. This allows the linking of gene expression to its biophysical consequences, thereby providing a dynamic, real-time framework for evaluating the roles of these genes in regulating cellular ion homeostasis and stress adaptation.

4.3 Abiotic stress alters energy allocation in *Aegiceras corniculatum* during chemical and physical responses, affecting its photosynthesis, growth, and adaptation

Abiotic stress remodels plant metabolism via energy sensing, diverting resources from growth towards stress tolerance [56, 57]. The ultimate energy source for plant growth and development is light energy [58]. High salinity and waterlogging environments can adversely affect the photosynthesis and growth of mangrove plants. In this study, the P_N of *A. corniculatum* at T3 treatment was 24.65% lower than that at T1 treatment, indicating a reduction in photosynthetic energy input. This energetic limitation was accompanied by impaired growth: stem elongation and leaf production (ΔH and ΔL_N) were both reduced at T3, consistent with *Kandelia candel* and *Bruguiera gymnorrhiza* responses [59]. In addition to chemical energy stored as ATP, a portion of the energy acquired via photosynthesis exists as dielectric motion in plant cells, defined here as cellular internal energy. With increasing stress intensity, relative cellular internal energy declined to approximately 50% of the T1 level. Photosynthetically derived chemical energy appears to support adaptive adjustments, whereas cellular internal energy is correlated with the capacity to support physical responses through its association with basal metabolic balance. This "photosynthesis-fueled stress resistance and cellular internal energy-stabilized metabolism" synergistic pattern ensures dynamic energy balance between chemical responses (e.g., ion balance, reactive oxygen species scavenging) and physical responses (e.g., turgor maintenance, ion transport, vacuolar compartmentalization). Even under severe stress and overall energy contraction, *Aegiceras corniculatum* appears to maintain a balance between "photosynthesis-internal-energy" and "growth-adaptability" through a relatively conserved allocation pattern, which likely contributes to basic survival and highlights the importance of these energy forms in its adaptive strategy.

In this study, T3 treatment notably boosted ATP levels, indicating that the chemical energy stored as ATP was less utilized. This suggests that the energy expended on actively expelling salt ions was significantly diminished.

Concurrently, T3 treatment substantially increased ΔG_{XC-E} and ΔG_{XL-E}, which correlate with the rise in LISAC and LISPIC. However, the ratio of ΔG_{XL-E} to ΔG_{XC-E} dropped from 97% at T1 to 80%. This can be attributed to two factors: firstly, the substantial reduction in compartmentalization ability due to severely shrunken vacuoles, and secondly, the internal energy for actively expelling salt ions is lower than that required for their passive influx. From these observations, it can be deduced that in response to high salinity and waterlogging, *A. corniculatum* allocates less energy to actively expel salt ions, using both chemical and internal energy, which leads to a reduction in its salt excretion capacity. These findings underscore the importance of both forms of energy for supporting plant survival and growth. The "Energy Reserve-Stress Resistance-Growth" model further reveals the directional energy allocation patterns: with increasing stress intensity, the relative growth-driving energy based on the d that supports growth-related processes consistently decreases, while the relative stress-response energy allocated to stress resistance significantly increases. This reflects a "sacrificing growth potential to enhance stress resistance" trade-off strategy.

5 Conclusion

This study elucidates the dynamics changes of water-salt transport in *Aegiceras corniculatum*, their close association with molecular mechanisms, and the dynamic patterns of energy allocation between growth and stress resistance. A key conclusion is that the expression of salt transport-related genes and water-salt transport dynamics form a coordinated response system that modulates active/passive salt transport, vacuolar compartmentalization efficiency,

cytoplasmic Na^+ concentration, and efflux processes, thereby contributing to a multi-dimensional defense system for plants to adapt to environmental stress. Specifically, saline-waterlogging stress significantly reduces the ratio of active to passive salt transport, impairs intracellular Na^+ transfer rate and transport capacity, and notably decreases the activities of *SOS1* and *NHX1*. Concurrently, it upregulates *VHAc1* expression and increases vacuolar H^+ concentration, which further disrupts the balance of vacuolar Na^+ compartmentalization. Preliminary evidence suggests that electrophysiology-based intracellular water-salt dynamic characteristics can serve as a reliable basis for validating the functions of key water-salt transport-related genes. Another key conclusion is that the essence of *Aegiceras corniculatum*'s adaptation to saline-waterlogging stress lies in the optimized allocation of energy resources—a dynamic balance between energy allocation to growth maintenance and that to stress-resistant dissipation. Chemical energy derived from photosynthesis (stored in the form of ATP) and internal energy (stored in the form of electrical energy) collectively underpin plant growth and environmental adaptability, with growth processes drawing primarily on internal energy. Notably, differences in adaptability determine variations in photosynthetic capacity. With increasing salinity and waterlogging duration, the plant allocates a greater proportion of energy to stress responses, thereby leading to growth restriction. In summary, by dissecting the complex interplay between water-salt transport dynamics and molecular regulatory mechanisms, and integrating observations of altered energy allocation patterns in *Aegiceras corniculatum* during chemical and physical responses under abiotic stress, this study provides deeper insights into the physiological and molecular mechanisms underlying its adaptation to harsh habitats—such as high salinity and waterlogging—at the land-sea interface.

Data Availability Statement

Data will be made available on request.

Funding

This work was supported by the Priority Academic Program Development of Jiangsu Higher Education Institutions under Grant PAPD-2023-87.

Conflicts of Interest

The authors declare no conflicts of interest.

AI Use Statement

The authors declare that generative AI was used solely for language translation during the preparation of this manuscript. Specifically, Doubao was used to assist with partial translation from Chinese to English. The authors reviewed and edited all AI-generated content to ensure accuracy, clarity, and consistency with the intended scientific meaning.

Ethical Approval and Consent to Participate

Not applicable.

References

[1] Osland, M. J., Chivoiu, B., Enwright, N. M., Thorne, K. M., Guntenspergen, G. R., Grace, J. B., & Swarzenzki, C. M. (2022). Migration and transformation of coastal wetlands in response to rising seas. *Science Advances, 8*(26). [CrossRef]

[2] Engels, J. G., Rink, F., & Jensen, K. (2011). Stress tolerance and biotic interactions determine plant zonation patterns in estuarine marshes during seedling emergence and early establishment. *Journal of Ecology, 99*(1), 277–287. [CrossRef]

[3] Islam, M. N., Bell, R. W., Barrett-Lennard, E. G., & Maniruzzaman, M. (2022). Growth and yield responses of sunflower to drainage in waterlogged saline soil are caused by changes in plant-water relations and ion concentrations in leaves. *Plant and Soil, 479*(1–2), 679–697. [CrossRef]

[4] Tahjib-Ul-Arif, M., Hasan, M. T., Rahman, M. A., Nuruzzaman, M., Rahman, A. M. S., Hasanuzzaman, M., & Brestic, M. (2023). Plant response to combined salinity and waterlogging stress: Current research progress and future prospects. *Plant Stress, 7*, 100137. [CrossRef]

[5] Zhang, Y., Liu, G., Dong, H., & Li, C. (2021). Waterlogging stress in cotton: Damage, adaptability, alleviation strategies, and mechanisms. *Crop Journal, 9*(2), 257–270. [CrossRef]

[6] Sandoval, M. N., Cirilo, A. G., Paytas, M. J., Zuil, S. G., & Izquierdo, N. G. (2024). Critical periods for waterlogging effects on yield and grain components in sunflower (Helianthus annuus), soybean (Glycine max) and sorghum (Sorghum bicolor): A comparative study. *Journal of Agronomy and Crop Science, 210*(5), e12765. [CrossRef]

[7] Zhang, R., Wang, Y., Hussain, S., Yang, S., Li, R., Liu, S., ... & Hou, H. (2022). Study on the effect of salt stress on yield and grain quality among different rice varieties. *Frontiers in Plant Science, 13*, 918460. [CrossRef]

[8] Foster, K. J., & Miklavcic, S. J. (2020). A comprehensive biophysical model of ion and water transport in plant roots. III. Quantifying the energy costs of ion transport in salt-stressed roots of Arabidopsis. *Frontiers in Plant Science, 11*, 865. [CrossRef]

[9] Takahashi, H., Abo, C., Suzuki, H., Romsuk, J., Oi, T., Yanagawa, A., ... & Nakazono, M. (2023). Triterpenoids in aerenchymatous phellem contribute to internal root aeration and waterlogging adaptability in soybeans. *New Phytologist, 239*(3), 936-948. [CrossRef]

[10] Craig Plett, D., & Møller, I. S. (2010). Na+ transport in glycophytic plants: what we know and would like to know. *Plant, cell & environment, 33*(4), 612-626. [CrossRef]

[11] Foster, K. J., & Miklavcic, S. J. (2015). Toward a biophysical understanding of the salt stress response of individual plant cells. *Journal of Theoretical Biology, 385*, 130–142. [CrossRef]

[12] Melkikh, A. V., & Sutormina, M. I. (2022). From leaves to roots: Biophysical models of transport of substances in plants. *Progress in Biophysics and Molecular Biology, 169*, 53-83. [CrossRef]

[13] Hasegawa, P. M. (2013). Sodium (Na+) homeostasis and salt tolerance of plants. *Environmental and Experimental Botany, 92*, 19–31. [CrossRef]

[14] Cubero-Font, P., & De Angeli, A. (2021). Connecting vacuolar and plasma membrane transport networks. *New Phytologist, 229*(2), 755-762. [CrossRef]

[15] Chen, J., Xiong, D. Y., Wang, W. H., Hu, W. J., Simon, M., Xiao, Q., ... & Zheng, H. L. (2013). Nitric oxide mediates root K+/Na+ balance in a mangrove plant, Kandelia obovata, by enhancing the expression of AKT1-type K+ channel and Na+/H+ antiporter under high salinity. *Plos one, 8*(8), e71543. [CrossRef]

[16] Chi, B. J., Guo, Z. J., Wei, M. Y., Song, S. W., Zhong, Y. H., Liu, J. W., ... & Zheng, H. L. (2024). Structural, developmental and functional analyses of leaf salt glands of mangrove recretohalophyte Aegiceras corniculatum. *Tree Physiology, 44*(1), tpad123. [CrossRef]

[17] Guo, Z., Wei, M. Y., Zhong, Y. H., Wu, X., Chi, B. J., Li, J., ... & Zheng, H. L. (2023). Leaf sodium homeostasis controlled by salt gland is associated with salt tolerance in mangrove plant Avicennia marina. *Tree Physiology, 43*(5), 817-831. [CrossRef]

[18] Wegner, L. H., & Shabala, S. (2020). Biochemical pH clamp: the forgotten resource in membrane bioenergetics. *New Phytologist, 225*(1), 37-47. [CrossRef]

[19] Sun, C. C., Chan, F. C., Ahamad, A., & Yao, Y. H. (2023). Improved Natural Plant Electrophysiology Sensor Design for Phytosensing System. *IEEE Transactions on Instrumentation and Measurement, 72*, 1-10. [CrossRef]

[20] Sukhov, V., Sukhova, E., & Vodeneev, V. (2019). Long-distance electrical signals as a link between the local action of stressors and the systemic physiological responses in higher plants. *Progress in Biophysics and Molecular Biology, 146*, 63–84. [CrossRef]

[21] Lopes, A. M., & Machado, J. T. (2014). Fractional order models of leaves. *Journal of Vibration and Control, 20*(7), 998-1008. [CrossRef]

[22] Buch-Pedersen, M. J., Pedersen, B. P., Veierskov, B., Nissen, P., & Palmgren, M. G. (2009). Protons and how they are transported by proton pumps. *Pflügers Archiv-European Journal of Physiology, 457*(3), 573-579. [CrossRef]

[23] Hmidi, D., Muraya, F., Fizames, C., Véry, A. A., & Roelfsema, M. R. G. (2025). Potassium extrusion by plant cells: evolution from an emergency valve to a driver of long-distance transport. *New Phytologist, 245*(1), 69-87. [CrossRef]

[24] Mohr, H., & Schopfer, P. (Eds.). (2012). *Plant physiology*. Springer Science & Business Media.

[25] Zhang, C., Wu, Y., Su, Y., Li, H., Fang, L., & Xing, D. (2021). Plant's electrophysiological information manifests the composition and nutrient transport characteristics of membrane proteins. *Plant Signaling & Behavior, 16*(7), 1918867. [CrossRef]

[26] Duan, R., Xing, D., Chen, T., & Wu, Y. (2022). Effects of different inorganic nitrogen sources of Iris pseudacorus and Iris japonica on energy distribution, nitrogen, and phosphorus removal. *HortScience, 57*(6), 698-707. [CrossRef]

[27] Fromm, J., & Lautner, S. (2007). Electrical signals and their physiological significance in plants. *Plant, cell & environment, 30*(3), 249-257. [CrossRef]

[28] Geng, Y., Wu, R., Wee, C. W., Xie, F., Wei, X., Chan, P. M. Y., ... & Dinneny, J. R. (2013). A spatio-temporal understanding of growth regulation during the salt stress response in Arabidopsis. *The Plant Cell, 25*(6), 2132-2154. [CrossRef]

[29] Julkowska, M. M., & Testerink, C. (2015). Tuning plant signaling and growth to survive salt. *Trends in Plant Science, 20*(9), 586–594. [CrossRef]

[30] Qie, Y. D., Zhang, Q. W., McAdam, S. A., & Cao, K. F. (2024). Stomatal dynamics are regulated by leaf hydraulic traits and guard cell anatomy in nine true mangrove species. *Plant Diversity, 46*(3), 395-405. [CrossRef]

[31] Wang, X., & Lu, C. (2024). Exploring the fast-growing mechanism of Laguncularia racemosa from the perspective of leaf traits and ultrastructure. *Aquatic Ecology, 58*(2), 387–398. [CrossRef]

[32] Gupta, A., Shaw, B. P., & Roychoudhury, A. (2021). NHX1, HKT, and monovalent cation transporters regulate K+ and Na+ transport during abiotic stress. *Transporters and Plant Osmotic Stress, 1–27*. Academic Press. [CrossRef]

[33] Quintero, F. J., Blatt, M. R., & Pardo, J. M. (2000). Functional conservation between yeast and plant endosomal Na+/H+ antiporters. *FEBS letters, 471*(2-3), 224-228. [CrossRef]

[34] Bassil, E., Tajima, H., Liang, Y. C., Ohto, M. A., Ushijima, K., Nakano, R., ... & Blumwald,

E. (2011). The Arabidopsis Na+/H+ antiporters NHX1 and NHX2 control vacuolar pH and K+ homeostasis to regulate growth, flower development, and reproduction. *The Plant Cell, 23*(9), 3482-3497. [CrossRef]

[35] Suzuki, N., Koussevitzky, S. H. A. I., Mittler, R. O. N., & Miller, G. A. D. (2012). ROS and redox signalling in the response of plants to abiotic stress. *Plant, cell & environment, 35*(2), 259-270. [CrossRef]

[36] Bandehagh, A., & Taylor, N. L. (2020). Can alternative metabolic pathways and shunts overcome salinity induced inhibition of central carbon metabolism in crops?. *Frontiers in Plant Science, 11*, 1072. [CrossRef]

[37] Silva, P., Façanha, A. R., Tavares, R. M., & Gerós, H. (2010). Role of tonoplast proton pumps and Na+/H+ antiport system in salt tolerance of Populus euphratica Oliv. *Journal of Plant Growth Regulation, 29*(1), 23-34. [CrossRef]

[38] Lang, T., Sun, H., Li, N., Lu, Y., Shen, Z., Jing, X., ... & Chen, S. (2014). Multiple signaling networks of extracellular ATP, hydrogen peroxide, calcium, and nitric oxide in the mediation of root ion fluxes in secretor and non-secretor mangroves under salt stress. *Aquatic Botany, 119*, 33-43. [CrossRef]

[39] Ouyang, X., Ma, J., Liu, Y., Li, P., Wei, R., Chen, Q., & Li, Y. (2023). Foliar cadmium uptake, transfer, and redistribution in Chili: A comparison of foliar and root uptake, metabolomic, and contribution. *Journal of Hazardous Materials, 453*, 131421. [CrossRef]

[40] Srikanth, S., Lum, S. K. Y., & Chen, Z. (2016). Mangrove root: adaptations and ecological importance. *Trees, 30*(2), 451-465. [CrossRef]

[41] Liu, H., An, X., Liu, X., Yang, S., Liu, Y., Wei, X., & Wang, J. (2024). Molecular mechanism of salinity and waterlogging tolerance in mangrove Kandelia Obovata. *Frontiers in Plant Science, 15*, 1354249. [CrossRef]

[42] Krauss, K. W., & Ball, M. C. (2013). On the halophytic nature of mangroves. *Trees, 27*(1), 7-11. [CrossRef]

[43] Gurovich, L. A., & Hermosilla, P. (2009). Electric signalling in fruit trees in response to water applications and light–darkness conditions. *Journal of plant physiology, 166*(3), 290-300. [CrossRef]

[44] Jócsák, I., Végvári, G., & Vozáry, E. (2019). Electrical impedance measurement on plants: a review with some insights to other fields. *Theoretical and Experimental Plant Physiology, 31*(3), 359-375. [CrossRef]

[45] Zhang, C., Wu, Y., Su, Y., Xing, D., Dai, Y., Wu, Y., & Fang, L. (2020). A plant's electrical parameters indicate its physiological state: A study of intracellular water metabolism. *Plants, 9*(10), 1256. [CrossRef]

[46] Ali Solangi, K., Wu, Y., Xing, D., Ahmed Qureshi, W., Hussain Tunio, M., Ali Sheikh, S., & Shabbir, A. (2022). Can electrophysiological information reflect the response of mangrove species to salt stress? A case study of rewatering and Sodium nitroprusside application. *Plant Signaling & Behavior, 17*(1), 2073420. [CrossRef]

[47] Repo, T., Zhang, G. A. N. G., Ryyppö, A., & Rikala, R. (2000). The electrical impedance spectroscopy of Scots pine (Pinus sylvestris L.) shoots in relation to cold acclimation. *Journal of Experimental Botany, 51*(353), 2095-2107. [CrossRef]

[48] Barnuevo, A., & Asaeda, T. (2018). Integrating the ecophysiology and biochemical stress indicators into the paradigm of mangrove ecology and a rehabilitation blueprint. *PLoS One, 13*(8), e0202227. [CrossRef]

[49] Shabala, S., Bose, J., & Hedrich, R. (2014). Salt bladders: do they matter?. *Trends in plant science, 19*(11), 687-691. [CrossRef]

[50] Parida, A. K., & Jha, B. (2010). Salt tolerance mechanisms in mangroves: a review. *Trees, 24*(2), 199-217. [CrossRef]

[51] Munns, R., & Tester, M. (2008). Mechanisms of salinity tolerance. *Annu. Rev. Plant Biol., 59*(1), 651-681. [CrossRef]

[52] Flowers, T.J., & Colmer, T.D. (2015). Plant salt tolerance: adaptations in halophytes. *Ann. Bot., 115*(3), 327-331. [CrossRef]

[53] Carden, D. E., Walker, D. J., Flowers, T. J., & Miller, A. J. (2003). Single-cell measurements of the contributions of cytosolic Na+ and K+ to salt tolerance. *Plant physiology, 131*(2), 676-683. [CrossRef]

[54] Britto, D. T., & Kronzucker, H. J. (2009). Ussing's conundrum and the search for transport mechanisms in plants. *New Phytologist, 243–246*.

[55] Kosová, K., Prášil, I. T., & Vítámvás, P. (2013). Protein contribution to plant salinity response and tolerance acquisition. *International journal of molecular sciences, 14*(4), 6757-6789. [CrossRef]

[56] Xu, Y., & Fu, X. (2022). Reprogramming of plant central metabolism in response to abiotic stresses: A metabolomics view. *International Journal of Molecular Sciences, 23*(10), 5716. [CrossRef]

[57] Rocha, A. G., & Vothknecht, U. C. (2012). The role of calcium in chloroplasts—an intriguing and unresolved puzzle. *Protoplasma, 249*(4), 957-966. [CrossRef]

[58] Jiang, B., Li, R., Shen, X., Zhang, Z., & Zhang, Y. (2022). Meta-analysis of mangrove salt-waterlogging tolerance and application strategies. *Acta Scientiarum Naturalium Universitatis Pekinensis, 58*(4), 687-699. [CrossRef]

[59] Ye, Y., Tam, N. F., Wong, Y. S., & Lu, C. Y. (2003). Growth and physiological responses of two mangrove species (Bruguiera gymnorrhiza and Kandelia candel) to waterlogging. *Environmental and Experimental botany, 49*(3), 209-221. [CrossRef]

Appendix

A Table of Nomenclature and Symbols

Symbol	Unit	Equation	Operational Definition
C	pF	$X_C = \frac{1}{2\pi fC}$	Physiological capacitance
Z	MΩ	/	Physiological impedance
R	MΩ	/	Physiological resistance
X_C	MΩ	/	Physiological capacitive reactance
X_L	MΩ	/	Physiological inductive reactance
ΔH	cm²	$\Delta H = H_A - H_B$	Plant height increment
ΔL_A	cm²	$\Delta L_A = L_{AA} - L_{AB}$	Leaf area increment
ΔL_N	count	/	Number of new leaves added
Ψ_L	MPa	/	Leaf water potential
IZ	-	$IZ = y_1 + k_1$	Inherent impedance
IR	-	$IR = y_2 + k_2$	Inherent resistance
IX_C	-	$IX_C = y_3 + k_3$	Inherent capacitive reactance
IX_L	-	$IX_L = y_4 + k_4$	Inherent inductive reactance
IC_P	-	$IC_P = \frac{1}{2\pi f \times IX_C}$	Inherent capacitance
d	-	$d = \frac{U^2 k_0}{2}$	Specific effective thickness
LIWHC	-	$LIWHC = (IC_P)^{3/2}$	Leaf intracellular water-holding capacity
LIWUE	-	$LIWUE = \frac{d}{LIWHC}$	Leaf intracellular water-use efficiency
LIWHT	-	$LIWHT = IC_P \times IZ$	Leaf intracellular water-holding time
LISAC	-	$LISAC = \frac{IX_L^{-1}}{IR^{-1}}$	Leaf intracellular salt active transport capacity per unit area
LISPC	-	$LISPCC = \frac{IX_C^{-1}}{IR^{-1}}$	Leaf intracellular salt passive transport capacity per unit area
LIUSF	-	$LIUSF = \frac{IR}{IX_C} + \frac{IR}{IX_L}$	Leaf intracellular salt flux per unit area
LISTR	-	$LISTR = \frac{(IC_P)^{\frac{3}{2}}}{(IC_P \times IZ)}$	Leaf intracellular salt transfer rate
LISTC	-	$LISTC = LIUSF \times LISTR$	Leaf intracellular salt transport capacity
ICC_{XC}	-	$ICC_{XC} = \frac{Ub_3k_3}{[(y_3+b_3)(y_3+b_3)]}$	Plant leaf inherent conduction capacity based on X_C
ICC_{XL}	-	$ICC_{XL} = \frac{Ub_4k_4}{[(y_4+b_4)(y_4+b_4)]}$	Plant leaf inherent conduction capacity based on X_L
ICR_{XC}	-	$ICR_{XC} = X'_{CF=0} = -b_3k_3$	Plant leaf inherent conduction resistance based on X_C
ICR_{XL}	-	$ICR_{XL} = X'_{LF=0} = -b_4k_4$	Plant leaf inherent conduction resistance based on X_L
ΔG_{Z-E}	-	$\Delta G_{Z-E} = \frac{\ln k_1 - \ln y_1}{b_1}$	Unit cellular internal energy based on Z
ΔG_{R-E}	-	$\Delta G_{R-E} = \frac{\ln k_2 - \ln y_2}{b_2}$	Unit cellular internal energy based on R
ΔG_{XC-E}	-	$\Delta G_{XC-E} = \frac{\ln k_3 - \ln y_3}{b_3}$	Unit cellular internal energy based on X_C
ΔG_{XL-E}	-	$\Delta G_{XL-E} = \frac{\ln k_4 - \ln y_4}{b_4}$	Unit cellular internal energy based on X_L
ΔG_Z	-	$\Delta G_Z = \frac{\ln k_2 - \ln y_2}{b_2} \times d_L$	Plant cellular internal energy based on Z
ΔG_R	-	$\Delta G_R = \frac{\ln k_1 - \ln y_1}{b_1} \times d_L$	Plant cellular internal energy based on R
ΔG_{XC}	-	$\Delta G_{XC} = \frac{\ln k_3 - \ln y_3}{b_3} \times d_L$	Plant cellular internal energy based on X_C
ΔG_{XL}	-	$\Delta G_{XL} = \frac{\ln k_4 - \ln y_4}{b_4} \times d_L$	Plant cellular internal energy based on X_L
P_N	μmol·m^{-2}·s^{-1}	/	Net photosynthetic rate
g_s	mmol·m^{-2}·s^{-1}	/ μ	Stomatal conductance
E	mmol·m^{-2}·s^{-1}	/ μ	Transpiration rate
WUE	μmol·mmol^{-1}	$\mathrm{WUE_i} = \frac{P_N}{E}$	Instantaneous water use efficiency
SOSl	-	/	PM Na^+/H^+ antiporter
NHXI	-	/	Vacuolar Na^+/H^+ antiporter
HAl	-	/	Plasma membrane H^+-ATPase
VHAcl	-	/	Vacuolar H^+-ATPase subunit c

B Derivation of Electrophysiological Parameters

B.1 The intrinsic mechanism relationship between clamping force (F) and leaf R, Z, X_C, X_L and C

The Nernst equation can be used to describe the changes in the concentration of ions, ion groups and electric dipoles inside and outside of the cell membrane. The Z depends on the concentration of ions inside and outside the membrane and follows the Nernst equation, which is expressed as follows:

$$E - E^0 = \frac{R_0 T}{n_Z F_0} \ln \frac{Q_i}{Q_0} \tag{A1}$$

where E is the electromotive force (V), E^0 is the standard electromotive force (V), R_0 is the gas constant (8.31 J·K^{-1}·mol^{-1}), T is the thermodynamic temperature (K), Q_i is the concentration of electrolytes that respond to Z inside the cell membrane (mol·L^{-1}), Q_0 is the concentration of electrolytes that respond to Z outside the cell membrane (mol·L^{-1}), F_0 is Faraday constant (9.65×10^4 C·mol^{-1}), and n_Z is the number of transferred electrolytes (mol).

The internal energy of the electromotive force can be converted into pressure work, and they have a direct relationship, $PV = aE$, that is:

$$PV = aE = aE^0 + \frac{aR_0 T}{n_Z F_0} \ln \frac{Q_i}{Q_0} \tag{A2}$$

where P is the pressure intensity on the leaf cells (Pa), a is the transfer coefficient from electromotive force to energy, and V is the cell volume (m^3). $P = \frac{F}{S}$, where F is the gripping force (N) and S is the effective area of the electrode plate (m^2). F can be calculated by the gravity formula:

$$F = (M + m)g \tag{A3}$$

where M is the iron block mass (kg), m is the mass of the plastic rod and the plate electrode (kg), and $g = 9.8$ N/kg.

For mesophyll cells, the sum of Q_0 and Q_i is certain. Q_i is directly proportional to the conductivity of electrolytes that respond to Z, and the conductivity is the reciprocal of Z. Hence, $\frac{Q_i}{Q_0}$ can be expressed as

$$\frac{Q_i}{Q_0} = \frac{\frac{J_0}{Z}}{Q - \frac{J_0}{Z}} = \frac{J_0}{QZ - J_0}, \tag{A4}$$

where J_0: the transfer coefficient between the Q_i and Z, and $Q = Q_0 + Q_i$. Therefore, formula (2) was transformed into formula (4):

$$\frac{V}{S} F = aE^0 - \frac{aR_0 T}{n_Z F_0} \ln \frac{QZ - J_0}{J_0} \tag{A5}$$

Formula (4) was rewritten:

$$\frac{aR_0 T}{n_Z F_0} \ln \frac{QZ - J_0}{J_0} = aE^0 - \frac{V}{S} F \tag{A6}$$

and

$$\ln \frac{QZ - J_0}{J_0} = \frac{n_Z F_0 E^0}{R_0 T} - \frac{V n_Z F_0}{S a R_0 T} F \tag{A7}$$

Formula (6) takes the exponents of both sides:

$$\frac{QZ - J_0}{J_0} = e^{\frac{n_Z F_0 E^0}{R_0 T}} e^{\left(-\frac{V n_Z F_0}{S a R_0 T} F\right)} \tag{A8}$$

Further:

$$Z = \frac{J_0}{Q} + \frac{J_0}{Q} e^{\frac{n_Z F_0 E^0}{R_0 T}} e^{\left(-\frac{V n_Z F_0}{S a R_0 T} F\right)} \tag{A9}$$

where the Z is the impedance, MΩ.

Because $d = \frac{V}{S}$, formula (8) was transformed into:

$$Z = \frac{J_0}{Q} + \frac{J_0}{Q} e^{\frac{n_Z F_0 E^0}{R_0 T}} e^{\left(-\frac{d n_Z F_0}{a R_0 T} F\right)} \tag{A10}$$

For the same leaf tested in the same environment, $d, a, E^0, R_0, T, n_Z, F_0, Q$, and J_0 of formula (8) are constant. Let

$$y_1 = \frac{J_0}{Q}, \quad k_1 = \frac{J_0}{Q} e^{\frac{n_Z F_0 E^0}{R_0 T}}, \quad b_1 = \frac{d n_Z F_0}{a R_0 T}, \tag{A11}$$

and the intrinsic mechanism relationships of leaf impedance (Z) and F were:

$$Z = y_1 + k_1 e^{-b_1 F} \tag{A12}$$

where y_1, k_1, and b_1 are model parameters.

The leaf physiological capacitive reactance (X_C) was calculated according to Formula (11):

$$X_C = \frac{1}{2\pi f C} \tag{A13}$$

The leaf physiological inductive reactance (X_L) was calculated according to Formula (12):

$$-\frac{1}{X_L} = \frac{1}{Z} - \frac{1}{R} - \frac{1}{X_C} \tag{A14}$$

With the same Z, the intrinsic mechanism relationships of leaf physiological resistance (R), X_C, X_L and F are revealed:

$$R = y_2 + k_2 e^{-b_2 F} \quad \text{(A15)}$$

$$X_C = y_3 + k_3 e^{-b_3 F} \quad \text{(A16)}$$

$$X_L = y_4 + k_4 e^{-b_4 F} \quad \text{(A17)}$$

The derivative of formula (10) is as follows:

$$Z' = -b_1 k_1 e^{-b_1 F} \quad \text{(A18)}$$

According to formula (10), when $F = 0$, the intrinsic impedance (IZ) of the plant leaves could be obtained:

$$IZ = y_1 + k_1 \quad \text{(A19)}$$

With the same IZ, when $F = 0$, the intrinsic resistance (IR), intrinsic capacitive reactance (IX_C), and intrinsic inductive reactance (IX_L) of plant leaves could be calculated as:

$$IR = y_2 + k_2 \quad \text{(A20)}$$

$$IX_C = y_3 + k_3 \quad \text{(A21)}$$

$$IX_L = y_4 + k_4 \quad \text{(A22)}$$

The intrinsic capacitance (IC_P) of plant leaves could also be obtained:

$$I_{C_P} = \frac{1}{2\pi f I X_C} \quad \text{(A23)}$$

where $\pi = 3.1416$, f: the frequency, and I_{XC}: the intrinsic capacitive reactance.

According to the first law of thermodynamics, the work done by the clamping force obeys the Gibbs free energy equation:

$$\Delta G = \Delta H + PV \quad \text{(A24)}$$

where ΔG: Gibbs free energy (J), ΔH: the internal energy of the leaf cell system (J), P: the pressure intensity of the leaf cells (Pa), and V: the cell volume (m^3). P can be calculated by the pressure intensity formula:

$$P = \frac{F}{S} \quad \text{(A25)}$$

where F: the clamping force (N) and S: the effective area of the electrode plate (m^2).

Mesophyll cells can be regarded as concentric sphere capacitors, and the capacitor energy is:

$$W = \frac{1}{2} U^2 C \quad \text{(A26)}$$

where W: the capacitor energy (J), U: the test voltage (V), and C: the physiological capacitance (pF).

According to energy conservation theory, the capacitor energy is equal to the work converted by Gibbs free energy, i.e., $W = \Delta G$. The leaf C and clamping force (F) relationship model was obtained:

$$C = \frac{2\Delta H}{U^2} + \frac{2V}{SU^2} F \quad \text{(A27)}$$

It is assumed that d represents the specific effective thickness of the plant leaves; therefore, $d = \frac{V}{S}$. Formula (24) was transformed into formula (26):

$$C = \frac{2\Delta H}{U^2} + \frac{2d}{U^2} F \quad \text{(A28)}$$

Let $y_0 = \frac{2\Delta H}{U^2}$, $k_0 = \frac{2d}{U^2}$, and formula (26) was transformed into formula (27):

$$C = y_0 + k_0 F \quad \text{(A29)}$$

Formula (27) is a linear model, where y_0 and k_0 are the model parameters.

As $k_0 = \frac{2d}{U^2}$, the specific effective thickness (d) of the plant leaves could be calculated as:

$$d = \frac{U^2 k_0}{2} \quad \text{(A30)}$$

B.2 Calculation of leaf intracellular water-holding capacity (LIWHC), leaf intracellular water-use efficiency (LIWUE), and leaf intracellular water-holding time (LIWHT)

The cell is a spherical structure, and its growth is closely related to the increased volume. The C of plant leaf cells can be calculated by a formula for concentric spherical capacitors:

$$C_C = \frac{4\pi\varepsilon R_1 R_2}{R_2 - R_1} \quad \text{(A31)}$$

where $\pi = 3.1416$, C_C: the capacitance of the concentric spherical capacitor (pF), ε: the dielectric constant of electrolytes, R_1: the outer sphere radius (m), and R_2: the inner sphere radius (m). For a plant cell, $R_2 - R_1$ is the thickness of the cell membrane. $R_1 \approx R_2$, as well as ε, and the thickness of the cell membrane is constant. Therefore, the cell volume (V_C) has the following relationship with cell's C:

$$V_C = \alpha\sqrt{C^3} \quad \text{(A32)}$$

The cell volume is positively correlated with the volume of vacuoles, and the main component of the vacuole and cytoplasm is water. In other words, the water-holding capacity of cells is directly proportional to $\sqrt{C^3}$. Therefore, $\sqrt{C^3}$ can represent the water-holding capacity of plant leaves. The leaf intracellular water-holding capacity (LIWHC) of plant leaves was obtained according to formula (30):

$$\text{LIWHC} = \sqrt{\text{IC}_P^3} \tag{A33}$$

The specific effective thickness (d) of plant leaves represents cell growth, and the water-holding capacity supports plant cell growth. Therefore, the leaf intracellular water-use efficiency (LIWUE) of leaves was represented by formula (32):

$$\text{LIWUE} = \frac{d}{\text{LIWHC}} \tag{A34}$$

According to Ohm's law, $I_Z = \frac{U}{Z}$, where I_Z: the physiological current (A). At the same time, the current is equal to the product of the capacitance and the differential of voltage in time, as shown in Formula (33):

$$I_Z = IC_P \times \int dU \tag{A35}$$

After the integral transformation, the current time is the product of C and Z. Therefore, the leaf intracellular water-holding time (LIWHT) of plant leaves is represented by Formula (34):

$$\text{LIWHT} = IC_P \times IZ \tag{A36}$$

B.3 Calculation of leaf intracellular salt active transport capacity (LISAC), leaf intracellular salt passive transport capacity (LISPC), leaf intracellular salt flux per unit area (LIUSF), leaf intracellular salt transfer rate (LISTR), and leaf intracellular salt transport capacity (LISTC)

Plant cells have the electrical properties of low C and high R, and it could be assumed that electrical cells were connected in parallel manner, and various aligned mesophyll cells make up the leaf capacitor. The value of IR in plant leaf cells can be measured as follows:

$$\frac{1}{\text{IR}} = \frac{1}{\text{IR}_1} + \frac{1}{\text{IR}_2} + \frac{1}{\text{IR}_3} + \frac{1}{\text{IR}_n} \tag{A37}$$

We can assume that the resistance of inside and outside membrane is equal; then, IR_1, IR_2, IR_3, and IR_n can represent inherent resistance of each unit cell membrane. Hence, the IR of the plant leaves were obtained as follows:

$$\frac{1}{\text{IR}} = \frac{n}{\text{IR}_0} \tag{A38}$$

Further, the R of the cell membrane closely related to lipids and proteins, so, n can be denoted as the relative number of lipids and proteins that induce membrane R in plant leaves.

Finally, the leaf IXC in plant were measured as follows:

$$\frac{1}{IX_C} = \frac{p}{IX_{C0}} \tag{A39}$$

As we know that X_C of cell membrane is closely related to the surface proteins, then IXC or p was considered as the relative amount of surface proteins. Therefore, IXC is inversely proportional to p.

$$\frac{1}{IX_L} = \frac{q}{IX_{L0}} \tag{A40}$$

As we know that X_L of cell membrane is closely related to the conjugated proteins, then IXL or q was considered as the relative number of conjugated proteins. Therefore, IXL is inversely proportional to q.

The cell membrane proteins are most closely related to salt transport. The proportion of phospholipids, surface proteins (peripheral proteins) and conjugated protein (intrinsic proteins) on the cell membrane strongly affects the transport capacity of cellular substances and ultimately affects the salt transport efficiency of plants.

Among, the leaf intracellular passive salt transport capacity (LISPT) is calculated as follows:

$$\text{LISPT} = \frac{p}{n} = \frac{\text{IX}_c^{-1}}{\text{IR}^{-1}} \tag{A41}$$

In addition, the proportion of conjugated protein (intrinsic protein) is closely related to the active transport of salt. The proportion of cell salt transport capacity caused by these proteins to total material transport capacity determines the leaf intracellular salt active transport capacity (LISAT). Therefore, the calculation formula is as follows:

$$\text{LISAT} = \frac{q}{n} = \frac{\text{IX}_L^{-1}}{\text{IR}^{-1}} \tag{A42}$$

Thus, the relative leaf intracellular salt flux per unit area (LIUSF) could be represented by (41):

$$\text{LIUSF} = \text{LISAT} + \text{LISPT} \tag{A43}$$

Salts are soluble in water; the leaf intracellular salt transfer rate (LISTR) is calculated by Formula (42):

$$\text{LISTR} = \sqrt{\frac{(\text{IC})^3}{\text{IC} \times \text{IZ}}} \tag{A44}$$

Therefore, the leaf intracellular salt transport capacity (LISTC) is LIUSF multiplied by LISTR:

$$\text{LISTC} = \text{LIUSF} \times \text{LISTR} \tag{A45}$$

B.4 Calculation of conduction capacity based on capacitive reactance (ICC_{XC}), conduction capacity based on inductive reactance (ICC_{XL}), conduction resistance based on capacitive reactance (ICR_{XC}), and conduction resistance based on inductive reactance (ICR_{XL})

According to Ohm's law, the physiological current $I_Z = U/Z$, where U is the measured voltage, $1.5\,\text{V}$, and I_Z is the physiological current. Therefore,

$$I_Z = \frac{U}{y_1 + k_1 e^{-b_1 F}} \tag{A46}$$

where I_Z is the physiological current with a measured voltage of $1.5\,\text{V}$. Taking the derivative of the above formula gives:

$$I'_Z = \frac{\partial I_Z}{\partial y_1} = \frac{U b_1 k_1 e^{-b_1 F}}{(y_1 + k_1 e^{-b_1 F})(y_1 + k_1 e^{-b_1 F})} \tag{A47}$$

The physiological current is generated by the movement of dielectric substances (including inorganic and organic ions) within leaves. This current reflects the conductivity of polar substances and is directly correlated with the leaf's hydraulic conductivity. The biological significance of conduction capacity based on physiological current can be characterized by the change of physiological current under unit pressure, representing the conductivity of leaves.

X_C reflects the ability to resist physiological currents. Similarly, when $F = 0$, the inherent conduction capacity of plant leaves based on IX_C (ICC_{XC}) was obtained:

$$ICC_{XC} = \frac{U b_3 k_3}{(y_3 + b_3)(y_3 + b_3)} \tag{A48}$$

Similar to ICC_{XL}, the inherent conduction capacity of plant leaves based on IX_L (ICC_{XL}) was obtained:

$$ICC_{XL} = \frac{U b_4 k_4}{(y_4 + b_4)(y_4 + b_4)} \tag{A49}$$

ICC_{XC} (ICC_{XL}) reflects the conductive capacity of capacitive (inductive) dielectric materials and the charging-discharging capability of cell membranes. A higher value indicates greater conductive efficiency of capacitive (particularly water) (inductive) dielectric materials, resulting in enhanced passive (active) membrane transport.

The Z of leaves reflects their ability to oppose physiological currents. As the Z increases, the transport of these substances slows down. Therefore, the Z of leaves can reflect the conductivity of polar substances in leaves from the opposite aspect, which is also the hydraulic conduction ability of leaves. The biological significance of the inherent conduction resistance of plant leaves based on Z can be characterized by the change of physiological impedance under unit pressure, representing the conductive resistance based on Z in leaves of the plant.

Similarly, according to the derivation formula of the relationship model between X_c and F:

$$X'_c = -b_3 k_3 e^{-b_3 F} \tag{A50}$$

The X_c of plant leaves reflects the ability to resist physiological currents, while physiological currents are generated by the transport of "capacitive" dielectric substances. The biological meaning of the above formula can be characterized as the change of X_c under unit pressure, which represents the conduction resistance of plant leaves based on X_c. When $F = 0$, the value is the inherent conduction resistance of plant leaves based on X_c (ICR_{XC}):

$$ICR_{XC} = Xc'_{F=0} = -b_3 k_3 \tag{A51}$$

Similar to X_c, according to the derivation formula of the relationship model between X_L and F:

$$X'_L = -b_4 k_4 e^{-b_4 F} \tag{A52}$$

The X_L of plant leaves also reflects the ability to resist physiological currents, while physiological currents are generated by the transport of "inductive" dielectric substances. Similarly, when $F = 0$, the value is the

inherent conduction resistance of plant leaves based on X_L (ICR_{XL}):

$$ICR_{XL} = X'_{LF=0} = -b_4 k_4 \tag{A53}$$

ICR_{XC} (ICR_{XL}) compares inherent conductance resistance in plant leaves based on physiological capacitance/resistance. A larger value suggests that capacitive (inductive) dielectric materials exhibit slower conductance rates and weaker passive (active) membrane transport capabilities.

B.5 Calculation of unit cellular internal energy and cellular internal energy

According to formula (10), the unit cellular internal energy based on Z (ΔG_{Z-E}) of plant leaves was calculated:

$$\Delta G_{Z-E} = \frac{aE^0}{d} = \frac{\ln k_1 - \ln y_1}{b_1} \tag{A54}$$

Similar to the derived formula for ΔG_{Z-E}, unit cellular internal energy based on R (ΔG_{R-E}), X_C (ΔG_{XC-E}) and X_L (ΔG_{XL-E}) is obtained.

$$\Delta G_{R-E} = \frac{aE^0}{d} = \frac{\ln k_2 - \ln y_2}{b_2} \tag{A55}$$

$$\Delta G_{XC-E} = \frac{aE^0}{d} = \frac{\ln k_3 - \ln y_3}{b_3} \tag{A56}$$

$$\Delta G_{XL-E} = \frac{aE^0}{d} = \frac{\ln k_4 - \ln y_4}{b_4} \tag{A57}$$

Cellular internal energy was calculated based on unit cellular internal energy and specific effective thickness (d), including cellular internal energy based on Z (ΔG_Z), cellular internal energy based on R (ΔG_R), cellular internal energy based on X_C (ΔG_{XC}), and cellular internal energy based on X_L (ΔG_{XL}). The formulas are as follows:

$$\Delta G_Z = \frac{\ln k_1 - \ln y_1}{b_1} \times d \tag{A58}$$

$$\Delta G_R = \frac{\ln k_2 - \ln y_2}{b_2} \times d \tag{A59}$$

$$\Delta G_{XC} = \frac{\ln k_3 - \ln y_3}{b_3} \times d \tag{A60}$$

$$\Delta G_{XL} = \frac{\ln k_4 - \ln y_4}{b_4} \times d \tag{A61}$$

Jing Wang holds an M.S. and a B.S. in Ecology. She is currently pursuing a Doctoral degree in Agricultural Resources and Environment at Nanjing Agricultural University. Her research focuses on plant stress resistance physiological ecology. She employs plant electrical biotechnology to explore the internal physiological status of mangrove leaf cells, providing technical support and theoretical references for the restoration practice of mangrove ecosystems. (Email: 2212216003@stmail.ujs.edu.cn)

Mohamed Aboueldahab is a PhD candidate in geochemistry at the University of Chinese Academy of Sciences, Institute of Geochemistry (Guiyang, China). His research integrates stable-isotope geochemistry, algal microbiology, and chromatography to investigate bicarbonate utilization and oxygen evolution in algae and karst waters. Previously, he served as a Demonstrator and Research Assistant at South Valley University (Qena, Egypt). He holds an M.Sc. in Microbiology (Phycology) and a B.Sc. in Chemistry & Microbiology from South Valley University, with additional training in water quality, advanced chromatography, and karst-ecosystem studies. (Email: mohamed@mail.gyig.ac.cn)

Yanyou Wu holds a Ph.D. in Botany, an M.S. in Plant Physiology and Biochemistry, and a B.S. in Biology. His research focuses on plant biophysics, electrobiology, and environmental adaptation. He has dedicated himself to explaining the fertility of certain intergeneric hybrids through "cell fusion- chromosome set segregation" and the extended genetic laws in his early years. He proposed a new mechanism of photosynthetic oxygen release: half of the oxygen originates from the photolysis of bicarbonate, and the other half from the photolysis of water. The release of oxygen through electrochemical energy is fundamental. He has also innovated plant electrobiological information detection technology and invented a plant life information instrument. Additionally, he created a technical method for characterizing physical information of life (including humans) based on the energy storage and conversion of cellular electrical components. He serves as the Editor-in-Chief of the Journal of Plant Electrobiology. (Email: wuyanyou@mail.gyig.ac.cn)

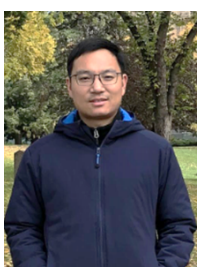

Deke Xing holds a Ph.D. in Geochemistry, M.S. in Agricultural Bioenvironment and Energy Engineering, and B.S. in Environmental Science. His research focuses on plant electrobiology, plant stress physiological ecology, and water-saving irrigation. He has successfully applied electrobiological techniques to research in plant stress physiological ecology and water-saving irrigation. By employing

advanced electrobiological monitoring and analytical methods, he investigated the dynamic characteristics of intracellular water utilization in various plant species under different environmental stresses, including drought and salinity conditions. Meanwhile, he developed quantitative models that correlate key electrobiological parameters with the plant's net photosynthetic rate and overall growth status, enabling the precise prediction and real-time assessment of both net photosynthetic rate and growth rate. These models have also been effectively applied to precision irrigation management, significantly improving water-use efficiency and sustainable agricultural practices. He currently serves as Associate Editor of the Journal of Plant Electrobiology. (Email: xingdeke@ujs.edu.cn)

Qian Zhang received her Master's degree in Ecology. Her primary research interests focus on plant electrophysiology and plant stress physiological ecology. She applies advanced electrophysiological techniques to rapidly and accurately monitor real-time changes in intracellular water dynamics in plant leaves under drought stress conditions. Her work aims to elucidate the relationship between dynamic intracellular water variations in leaves and the overall plant water status, as well as their effects on key physiological indicators. (Email: 2212216008@stmail.ujs.edu.cn)